Technical Report

392

E. J. Chatterton

Optical Communications Employing Semiconductor Lasers

9 June 1965

Lincoln Laboratory

MASSACHUSETTS INSTITUTE OF TECHNOLOGY

Lexington, Massachusetts
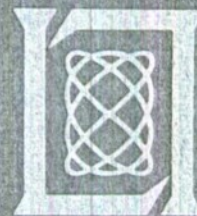
ESRL

AD0630243

MASSACHUSETTS INSTITUTE OF TECHNOLOGY

LINCOLN LABORATORY

OPTICAL COMMUNICATIONS
EMPLOYING SEMICONDUCTOR LASERS

E. J. CHATTERTON

Group 82

TECHNICAL REPORT 392

9 JUNE 1965

LEXINGTON   MASSACHUSETTS

ABSTRACT

This report discusses the development of optical communications employing semiconductor lasers — both noncoherent and coherent. The large modulation bandwidth obtainable with these devices permits the development of frequency- and pulse-modulation communications systems which overcome scintillation noise produced by the turbulent atmosphere. Emphasis has been placed on the development of communications systems for 98-percent weather capability over short ranges, rather than fair-weather capability over long ranges. The development of supporting technology is presented in the areas of semiconductor lasers, fiber optics, optical systems, narrow-band optical filters, photomultipliers, and frequency- and pulse-modulation electronic circuitry and components.

Measurements of optical signals over a two-mile path under a full variety of weather conditions have permitted a comparative evaluation of AM, FM, and PM systems. The results show clearly the advantage of frequency modulation and pulse modulation. Measurements of pulses transmitted appreciably beyond the limits of visibility in snow and fog indicate a channel bandwidth, limited by scatter-multipaths, but of the order of 200 Mcps.

An analysis is presented of multiple-scatter paths and system design considerations for these conditions.

The technology is described for combining the outputs of arrays of semiconductor lasers through fiber optics. Applications of the technology are discussed for (1) high-power, pulse-modulation systems, (2) time-, frequency-, and wavelength-multiplexing systems, (3) very-high-resolution optical television systems, and (4) electronically scanned laser systems.

TABLE OF CONTENTS

OPTICAL COMMUNICATIONS
EMPLOYING SEMICONDUCTOR LASERS

I. INTRODUCTION

Since the first published report of noncoherent radiation by GaAs[1] diodes and the subsequent announcements of coherent laser activity in GaAs[2] and other materials,[3] there has been much interest in the application of lasers to optical communications systems.[4] The characteristics of these devices which originally stimulated interest in communications applications and have remained competitively attractive in the face of equally rapid development in fields of gas and solid laser technology and various modulator technologies are:

> Intense radiance
>
> Narrow spectral emission which permits discrimination against background and foreground sources
>
> Efficiency of energy conversion
>
> Exceedingly small-time constants and the ease with which wide-band modulations can be effected electronically.

Equally appreciated have been two limitations in the use of these devices in communications:

> Small size and hence small power
>
> Cryogenic requirements.

However, recent laser developments,[5] which involve increased size and power, less stringent cryogenic requirements, progress in cryogenic technology, and the work in multiple-laser arrays reported here, incur optimism.

The coherent properties of lasers which exhibit or permit the attainment of very narrow beamwidths will have value in space systems. However, the work reported here has been directed toward the more immediate problem of optical communications through nonvacuum, real and noisy atmospheric channels. Under these conditions, very narrow beamwidths lose value as will be shown, and thus, interest in coherent properties per se is diminished. In this view, the inferiority of presently available semiconductor lasers compared to some gas and solid lasers in their property of diffraction limited beamwidth (which is related to minimum beamwidth attainable by use of external optics) is of no basic consequence.

Our emphasis has been placed on developing semiconductor laser communications systems for "all-weather" capability over short ranges, rather than for long-range but only fair-weather capability. By "all weather" we mean "relatively all weather." We are not addressing the heaviest fog conditions, nor are we considering such high-powered lasers as might interact with the medium to coalesce or evaporate a tunnel through the fog. We are concerned with the spectrum of atmospheric limitations to optical propagation between the extremes. In general,

we shall be interested in atmospheric limitations imposed by turbulence, absorption, and scatter. It was obvious from the start that what could be accomplished depended strongly on how much excess optical power was available for overcoming the atmospheric limitations. Therefore, while the twofold objectives were to

> Explore the nature of the atmospheric limitations and
>
> Evaluate various forms of modulation in their effectiveness in overcoming the limitations,

it was also necessary to

> Develop supporting technology in order to attain sufficient signal power to pursue the primary objectives.

Because we are working in a new field, the development of supporting technology has taken most of the time and effort. Accordingly, this report reflects those developments wherever they were appreciably beyond the existing state-of-the-art.

The report begins with the preliminary investigations of frequency modulation of optical signals reported earlier.[6] The development of technology to permit comparative evaluations of AM and FM techniques in the field and the results of those tests are presented in Secs. III, IV, and V. These developments and tests employed the noncoherent GaAs diodes.

When GaAs lasers became available, our work moved on to the more sophisticated pulse modulation systems. The development efforts and results of field tests with PM systems are given in Secs. VI, VII, and VIII.

Appendix A presents an analysis of communications through multiple-scatter atmospheric paths and system design considerations for these conditions.

Appendix B discusses applications of the technology reported herein, based on the feasibilities demonstrated by the analyses, laboratory tests, and field measurements.

II. ATMOSPHERIC LIMITATIONS TO OPTICAL COMMUNICATIONS

Our applied research of optical communications contended immediately with atmospheric limitations and was pursued from the outset within the notion of engineering compromise among factors of range, channel capacity, and operational duty time permitted by weather conditions.

The mechanisms of atmospheric limitations are many and varied. Attenuation through an atmospheric path may be expected from:

> Scattering by atmospheric molecules (Rayleigh scattering)
>
> Selective molecular absorption by H_2O, CO_2, O_2, O_3, and some other minor constituents
>
> Scattering and absorption by aerosols such as haze, dust, fog, clouds, and smog (probably a combination of small-particle Rayleigh scattering and large-particle Mie scattering)
>
> Refraction and dispersion by inhomogeneities in atmospheric composition, density, and index of refraction.

Any or all of these mechanisms contributing to attenuation will also contribute to the problem of signal-to-ambient discrimination, by their intervening action on celestial and man-made sources, causing both background and foreground ambient illumination.

Fluctuations in the density and index of refraction of the atmosphere resulting from turbulence will induce additive channel noise on the ambient illumination components and multiplicative noise

(shimmer, scintillations) on the signal components. These scintillations or modulation noises vary in direct proportion to the optical signal amplitude and, therefore, cannot be overcome by sufficient signal strength as can the ambient and receiver additive noises.

Consider the effect on a light ray impinging on a single turbulon which has a density slightly different from the density of the homogeneous media in which it is immersed. The light ray will suffer some angular dispersion because of the weak lens effect of the turbulon surfaces and also some retardation or advance in time of propagation through the turbulon relative to a ray in the homogeneous media. In the dynamic situation of many turbulons of different sizes, shapes, and densities, the effect on a beam of light will be an amplitude modulation resulting from fluctuating angular dispersion and a transit-time dispersion resulting from fluctuating velocity-of-propagation. For the special case of a coherent laser beam, we can speak of the transit-time dispersion in terms of phase modulation of the coherent optical wave.

The degree of amplitude and phase modulation imparted to an optical signal will depend not only on the turbulence characteristics of the media but also on the geometry of the path, as defined by source aperture and beamwidth, pathlength, and receiver aperture.[7,8,9] This dependency can be seen by considering an optical path having the geometry of a truncated cone. For the case in which the receiver aperture is smaller than the cross section of the projected laser beam, the ends of the path cone are defined by the apertures of the transmitter and receiver optics. Scintillation noise will be impressed on the beam by turbulons of varying density which traverse the path cone. Those turbulons smaller than the cone diameter and nearer the smaller end of the cone will occlude a larger percentage of the total beam, causing correspondingly more modulation noise. Similarly, paths of smaller diameter throughout their length incur more modulation noise.

The seriousness of transit-time dispersion depends largely on which characteristic of the laser beam is chosen to convey the information content. Systems such as the optical heterodyne type, wherein the information content is conveyed in modulation side bands about a coherent optical carrier, will suffer when the phase modulations imparted to different portions of the beam impinging on the receiver aperture amount to a fraction of a wavelength of the optical carrier. This amounts to differences in total pathlength within the beam, which result from fluctuating inhomogeneities, of a fraction of a micron. On the other hand, systems in which information signal detection is not dependent on maintenance of optical coherency over the path will be limited only when the transit-time dispersion approaches the period of the highest information signal or subcarrier frequencies. It is not obvious what effect, if any, scintillation noise will have on systems in which the information content is conveyed on the polarization of the optical carrier. This area appears worthy of further consideration.

The absorptive, scattering, refractive, and diffractive factors of the atmosphere and their fluctuations will set limits on minimum attainable beamwidth and pointing ability. Refraction (displacement) and diffraction (dispersion) of the laser beam will occur even in clear-air paths because of turbulons of varying size and index of refraction within the path geometry, the path volume closest to the source being most important. The varying index of refraction of the turbulons is a direct consequence of their varying temperature which produces varying density. For ground communications through the terrain-atmosphere turbulent layer, the intensity of the fluctuations is a function of the heat exchange dynamics between the air and the terrain, which, in turn, depends on height above the terrain, the immediate terrain topography in relation to adjacent topography, time of day or night, meteorological conditions, etc.
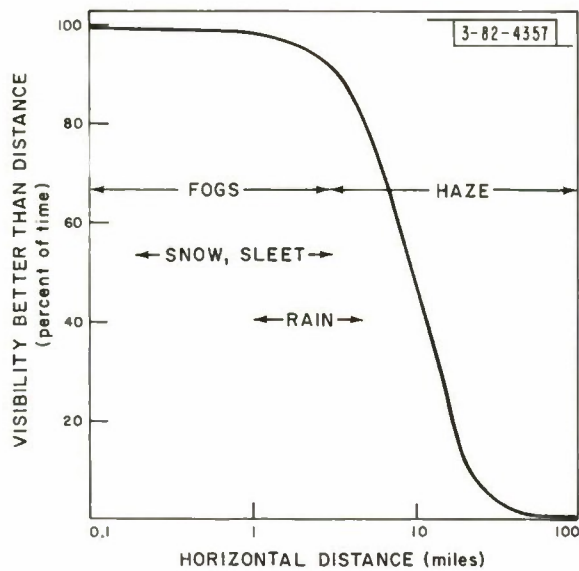
3

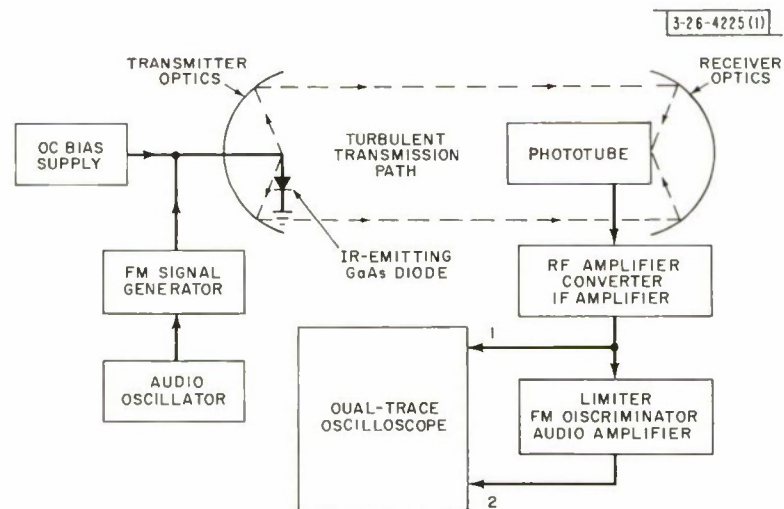Fig. 1. Visibility characteristic. Estimated for inland New England weather.

Fig. 2. FM optical communications system.

For earth-to-space transmissions, the turbulent tropopause region is a path volume of major importance, in addition to the terrain-atmosphere turbulent region, for its effect on minimum attainable beamwidth and scintillation noise. Space-to-earth beamwidth limitation is related to the astronomy problem of minimum resolution limited by "seeing" conditions. Since the atmospheric disturbances are close to the receiver in the astronomy case, appreciably better angular resolution can be achieved than the minimum transmitted beamwidths that can be achieved in the reverse direction.

Finally, multiple scattering by particles within atmospheric paths will set limits on channel bandwidths because of transit-time dispersion. An analysis of this most important limitation is given in Appendix A.

To help assess the atmospheric limitations for order of importance for ground communications, consider Fig. 1 which depicts a plot of the percentage of time that visibility is better than a given distance. This characteristic is roughly estimated for year-around, inland, New England weather. Coastal locations would experience shorter visibility distances, and desert locations would experience longer visibility distances. It is conservative to expect an optical communications system to achieve an operational duty time vs distance at least as good as visibility characteristics for that location. It is reasonable to pursue an operational range several times the visibility range.

System designs directed to 50-percent operational duty time over 25- to 50-mile relatively clear-air paths (New England weather), such as systems for "store and forward" of low priority messages on heavy traffic routes, will have to contend primarily with absorption and scatter of molecules, low density aerosols of haze and dust, and all effects of turbulence and multiple scatter. System designs directed to 98-percent operational duty time over 5- to 10-mile paths must contend primarily with absorption and scatter of fogs, snow, and rain, and all effects of turbulence and multiple scatter. In the 25- to 50-mile clear-weather system, refraction and dispersion effects of the atmosphere on minimum achievable beamwidths will limit receiver signal strength, turbulence will limit signal-to-noise ratio, and transit-time dispersion by turbulence and small-particle scatter will limit channel bandwidth. In the 5- to 10-mile 98-percent weather system, signal strength and channel bandwidth will be limited by multiple scatter of large particles, and turbulence will limit signal-to-noise ratio. Both systems must contend with ambient illuminations.

III. LABORATORY EXPLORATION OF FM OPTICAL SYSTEM

Early investigation of optical communications systems indicated that a major limitation on range and operational duty time under a variety of weather conditions was scintillation modulation introduced by the turbulent atmosphere. The large modulation bandwidths obtainable with the, then recently available, semiconductor IR emitting diodes suggested the use of FM and PM techniques to overcome scintillation noise.

A block schematic of the initial laboratory system is shown in Fig. 2. The transmitter employed a liquid nitrogen cooled GaAs diode emitting noncoherently. The diode was forward biased with DC and amplitude modulated by a 30-Mcps subcarrier. The subcarrier was frequency modulated (5-kcps deviation) by an audio signal. The receiver consisted of a photomultiplier tube which fed directly into the antenna input of an FM communications receiver. Crude optics sufficed for this preliminary evaluation. The system was operated across a laboratory

5

and modulation noise was induced in the transmission path by a variety of expedients (bubbling liquid nitrogen, fans, smoke, water spray, paper strips and fan blades directly in the path). Figure 3 shows the value of the FM technique in overcoming the induced modulation noise. The top trace of the oscilloscope monitored the IF signal of the FM communications receiver and was indicative of the incident radiation at the receiver aperture. The bottom trace monitored the audio output.
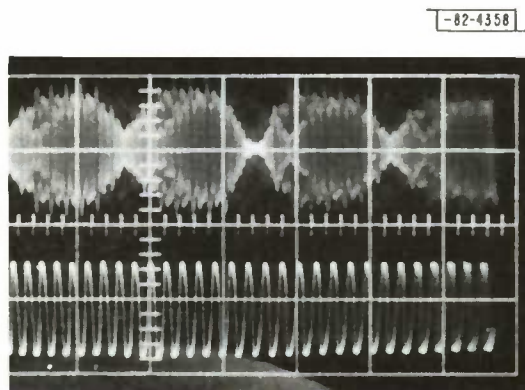

Fig. 3. FM optical signal. Upper trace: receiver IF signal. Lower trace: receiver audio output.

It is noted that the FM technique eliminated amplitude modulations, as high as 90 percent, originating in the transmission path. This laboratory exploration of the FM technique led to the pursuit of a field exploration under a variety of weather conditions.

IV. DEVELOPMENTS FOR AM AND FM OPTICAL COMMUNICATIONS

A number of developments in supporting technology were necessary in order to evaluate modulation techniques under a variety of atmospheric conditions. The following section describes these considerations and developments.

A. Field Sites and Optical Path

The choice of pathlength was dictated by two considerations:

(1) In view of the very limited power capability of the available IR emitting diodes, shorter paths would afford more signal strength which could be traded off with techniques for investigating and overcoming atmospheric limitations.

(2) The paths should be several times longer than visibility ranges that occur in poor weather to enable exploration of multiple-scatter conditions.

In accord with these considerations, together with estimates of local visibility characteristics, a nominal pathlength of 2 miles was chosen. Since a study of turbulence effects was to be emphasized, a path wherein the terrain-atmospheric layer was expected to be particularly dynamic and varied was highly desired. Logistic considerations dictated locating at least one terminal in our laboratory area. A folded path by means of mirrors, thus permitting both terminals to be within the laboratory area, was considered. However, this was rejected because (1) a path folded back upon itself by means of a large retro-mirror would introduce unresolvable effects of backscatter, and (2) the alignment and sufficiently rigid mounting problems of large plane mirrors in a triangular path appeared too difficult.

6

The path chosen was 1.8 miles long located across Hanscom Field, between a penthouse on the Lincoln Laboratory building and a trailer on the grounds of the M.I.T. Instrumentation Laboratory. A photograph of the view along the path from the penthouse toward the trailer is shown in Fig. 4. The path ranges from 45 to 8 feet above ground level and passes over a terrain studded with buildings and airport runways and aprons. The receiver faces west, a direction of relatively larger ambient illumination during the day. At nighttime the general area under the path is illuminated by a great number of street, building, and flood lights. The trailer transmitter site and the receiver penthouse terminal are shown in Figs. 5 and 6, respectively.

Logistic arrangements provided for personnel access on a 24-hour day, 7-day week basis as required by the infrequency and short duration of sufficiently poor weather conditions.

B. Meteorological Data

For evaluation of the merits of various forms of modulation under a variety of atmospheric conditions, it appeared desirable to record quantitatively the various pertinent meteorological parameters. Pertinent data on the gross meteorological parameters, such as temperature, relative humidity, wind direction and speed, amount of precipitation, and visibility, were readily measurable or available from the Hanscom Air Weather Service.

The highly variant visibility under conditions of fogs and snow required our own immediate estimate during measurement periods. A number of foreground and background lights served this purpose well at night, not so much as a quantitative measurement of visibility but as a relative measure within the 2-mile path which afforded comparisons among different tests. The lights that were chosen and consistently used were two blinking amber traffic lights at 0.3 and 0.6 mile, a building light at 1.1 miles, a 250-watt light at the trailer site (1.8 miles), and street lights at 2.0 miles. Although ambient illumination at night in fog was high, our criterion is believed to specify visibility distances somewhat greater than the common use of the term would indicate.

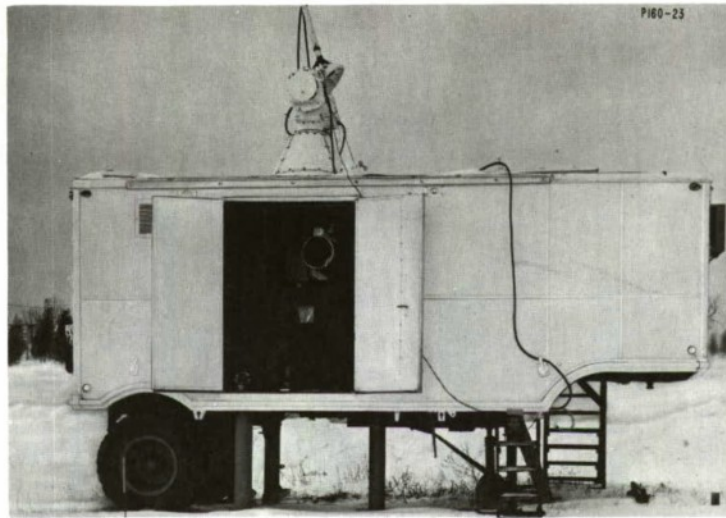Fig. 4. View along two-mile optical path.
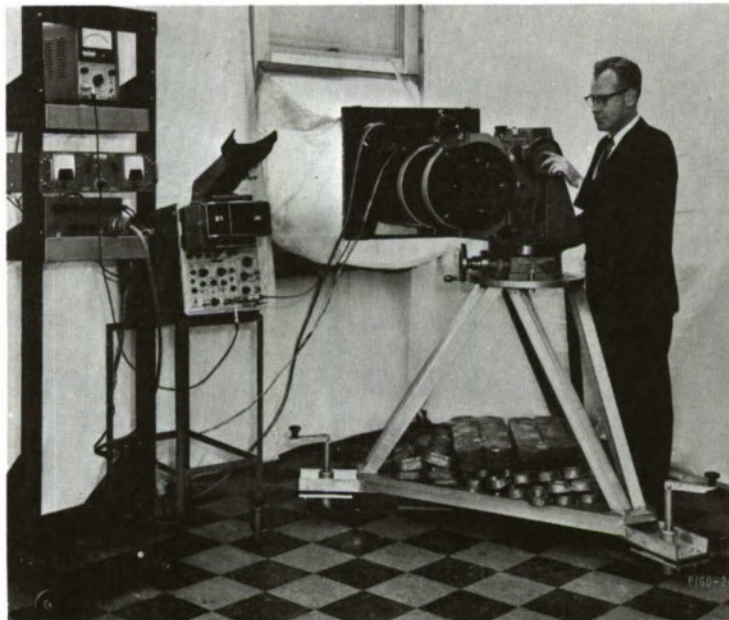
Fig. 5.   Trailer field site.

Fig. 6.   Penthouse terminal showing telescope and mount.

The recording of micrometeorometric data, particularly microthermometric data, was considered the best means for characterizing turbulence. These data appeared desirable to ensure that scintillation noise measurements made at different times using different modulation techniques were comparable. However, the cost and effort of recording these data were avoided, with some diminution in the research scope of the program, by making essentially simultaneous measurements with both FM and AM techniques.

C. Telescope Systems

Telescope systems were designed and constructed with emphasis on large apertures in view of the constant drive for higher powers and better sensitivities; rugged, nonmicrophonic construction to ensure validity of scintillation noise measurements; large, versatile and accessible design to permit a great variety of sources, sensors, and accommodations for specialized experimentation.

A high degree of ruggedness was required to ensure against microphonics which could not be distinguished from scintillation noise caused by turbulence in the atmospheric path. A high degree of long-term pointing stability was essential for operations during weather conditions when visibility was less than the pathlength. In general, every practical effort was made to ensure that the basic telescope systems would serve as a test bed for a long-term and varied program of optical propagation research and communications development. Both the basic transmitter and receiver telescopes were identical.

Primary optics consisted of 10-inch F/1.3 spherical reflective lenses which were aluminized and coated. Calibrated variable iris and shutter apertures were provided. A variety of secondary optics and apertures associated with the laser or photomultiplier tube assemblies completed the optics system.

Elevation and azimuth controls of the telescopes were effected by means of two heavy-duty rotary tables as shown in Fig. 6. Sighting was provided by 16-power Wollansak spyglasses. The telescopes were mounted on rugged pedestals which in turn were mounted on three jacks. The jacks passed through holes in the floor and rested on firm foundations. In the case of the penthouse terminal, a firm foundation was provided by 12-inch I-beams resting directly on the building piers. At the trailer site (Fig. 5) a 4-foot-deep concrete pier in the ground under the trailer and 6-inch-diameter steel pipes filled with concrete provided a firm foundation for the telescope mounts. Both mounts were loaded with 1000 pounds of lead.

The rugged construction and the precision of the rotary tables permitted pointing accuracy, stability, and repeatability of 0.1 mrad under all conditions except high winds. Long-duration 30-mph gusts caused the entire building to deflect slowly 0.16 mrad. Deflection of the transmitter telescope at the trailer site by gusts was undetectable (less than 0.05 mrad).

Boresighting of the receiver telescope with its sighting scope was effected by using a distant street light as a target. Boresighting of the transmitter was accomplished by locating the laser beam with the aid of a snooperscope at a distance of 50 feet, making gross corrections to boresighting, then progressing to greater distances and making finer adjustments.

D. Nitrogen Dewar for Noncoherent IR-Emitting Diodes

A nitrogen dewar was designed to accommodate a variety of IR GaAs diodes, having different sizes and shapes, and to be suitable for both laboratory evaluations of the diodes and for use in the

field telescope. The latter use required nonmicrophonic construction. In particular, it was necessary to maintain the emitting side of the diode free from bubbling nitrogen which would introduce modulation noise indistinguishable from atmospheric scintillation noise. The dewar (Fig. 7) is of double-wall design and fabricated from helio-arc welded stainless steel. The dewar window, vacuum sealed with an O-ring, may be detached, permitting removal of interchangeable cartridges containing different diodes. A nitrogen-temperature vacuum seal to the cartridge was effected by a soft copper washer. Each diode package was soldered into a cartridge so that its back was in contact with liquid nitrogen and its window was in vacuum. A coaxial line feed to the diode led through the nitrogen reservoir. The $1\frac{1}{2}$-liter capacity provided cooling for more than one hour.

E. Evaluation of Noncoherent IR Diodes

The IR GaAs diodes, which were procured from several sources, included a Lincoln Laboratory model.

Measurements were made of comparative IR output, spectral emission vs current, and I-V characteristics, all at liquid nitrogen temperature. Since the state-of-the-art is developing
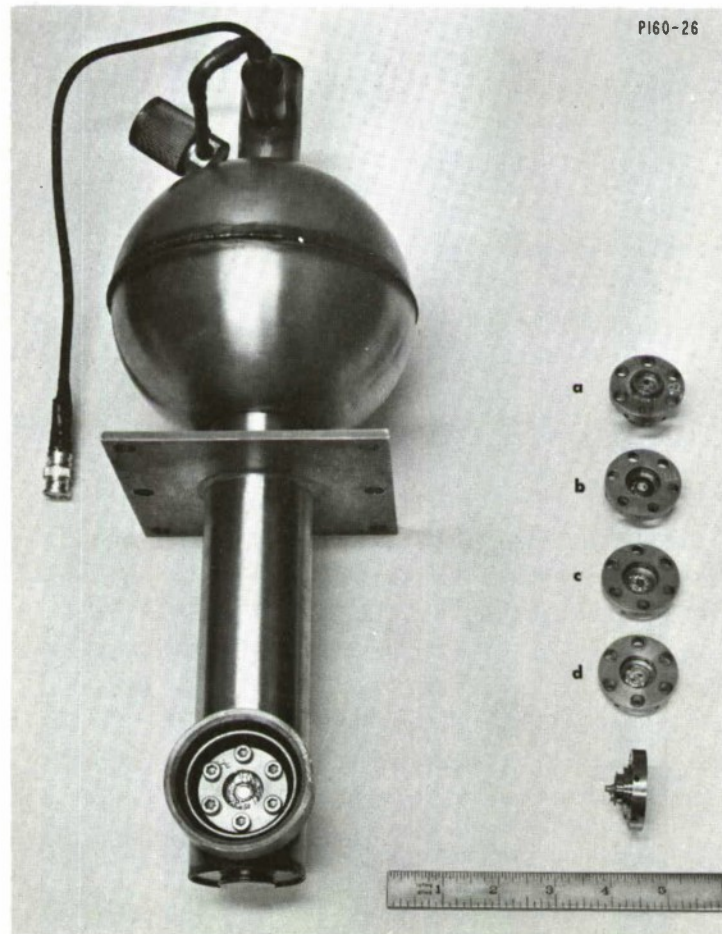
Fig. 7. Nitrogen dewar.

rapidly, our comparative measurements of over a year ago are probably not pertinent today. At the time, however, a commercially available type was selected for field use.

Since the application required as much IR power as possible, the junction temperature rise and consequent increase in wavelength with drive was important. Figure 8 shows this characteristic for two diodes. The half-power spectral bandwidth of these units was 240 Å and did not change significantly with current. Output power was nearly linear with current and measured 8 mw at 4 amp.

The I-V characteristic (see Fig. 9) provides design information for optimum DC bias current, maximum RF currents for linearity, and DC and RF impedances. However, it was found in practice that by setting the bias current equal to or somewhat lower than the peak RF current, the nonlinearities introduced on the RF subcarrier incurred no distortion of the signal upon detection. The lower DC dissipation permitted higher RF drives and signal output. A minimum DC bias was necessary to prevent exceeding the diode's back voltage rating on negative excursions of the carrier.

F. Narrow-Band IR Filters

Narrow-band IR filters are necessary to discriminate against ambient illuminations. Filters are readily available from several suppliers with wave-pass characteristics specified to match the spectral emission characteristics of specific GaAs diodes at their rms operating point (see Figs. 8 and 9). These interference-type filters are quite sensitive to angle-of-incidence, as shown in Fig. 10(a-b), and shift to lower wavelengths for increased angle of incidence. Bandwidth increases erratically with incidence angle. The filters perform well in optical systems having F-numbers greater than F/5.6 (5-degree maximum incidence angle) but become very inefficient in F/1.3 systems (23-degree maximum incidence angle).

One solution to the problem is the use of a secondary lens to collimate the flux before transmission through the filter. Figure 11 includes a sketch of this arrangement. The secondary
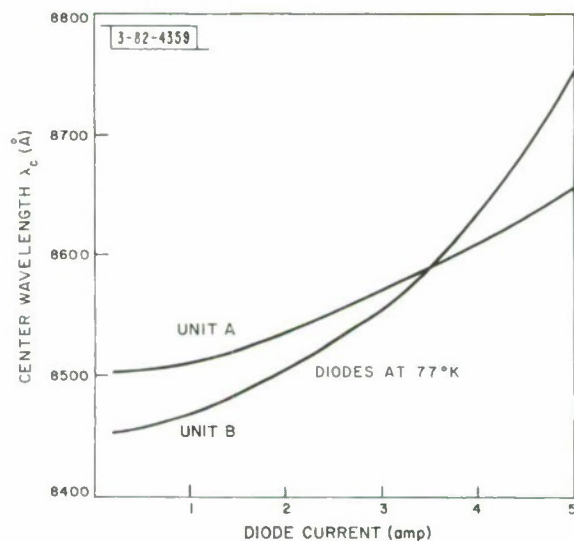

Fig. 8.   Infrared diode wavelength characteristics.
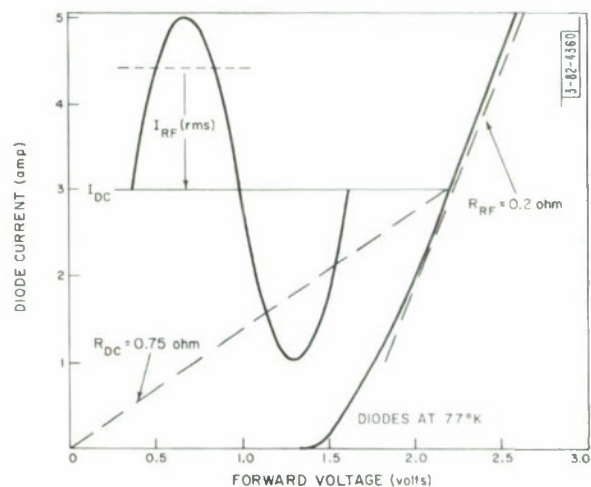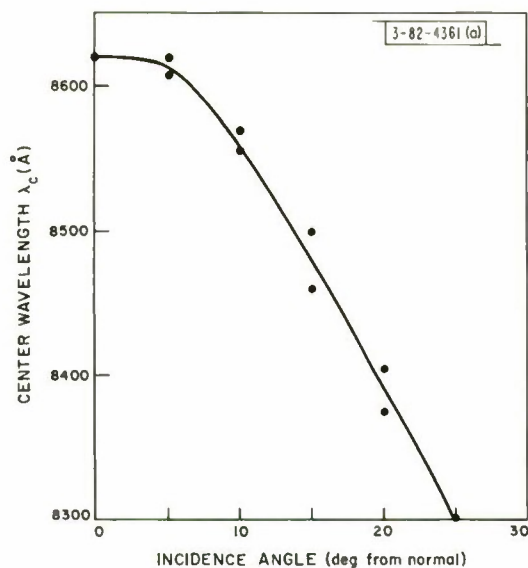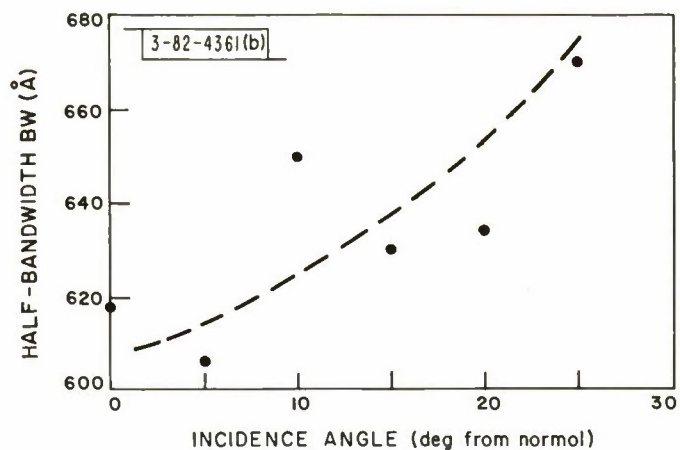

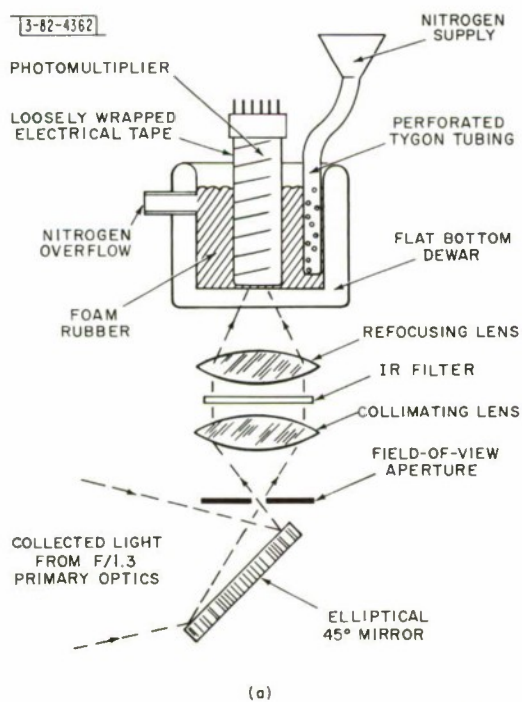Fig. 9.   Infrared diode I-V characteristic.

(a) Wovelength vs incidence angle.

(b) Bandwidth vs incidence angle.

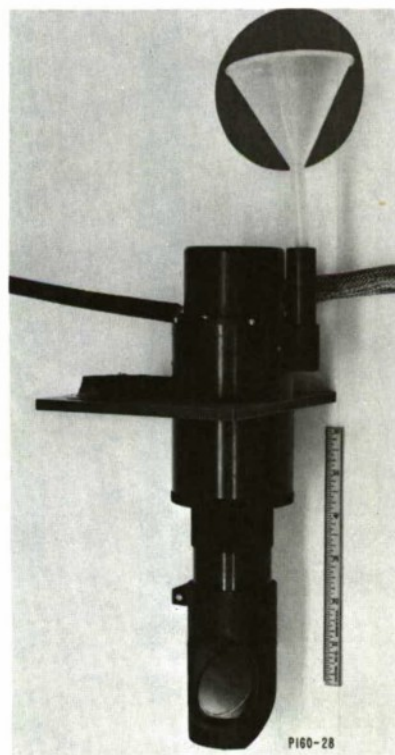Fig. 10(a-b). Infrared filter characteristics.

(a)

Fig. 11(a-b). Cooled photomultiplier assembly.

F-number must be equal to or smaller than the primary F-number. The design is good only for narrow field-of-view systems because of the angular magnification of the two-lens system:

$$\frac{\text{field-of-view}}{2} = \text{maximum filter incidence angle} \times \frac{\text{secondary diameter}}{\text{primary diameter}}$$

For the designed system, restricted to use of 1-inch-diameter filters, the field-of-view with the 10-inch primary was limited to 1 degree.

For maximum signal strength under dense scatter conditions, where fields-of-view up to 10 degrees are desired,[*] there are several solutions:

> Employ a filter which is deposited on a spherical-segment substrate. This construction is presently beyond the state-of-the-art.

> Cover the primary aperture with a mosaic of filters. This solution is expensive ($90 per square inch).

> Use telescopes having F-numbers of F/5.6 or greater. This solution adds greatly to size or complexity of the optics system. Of course, as more powerful lasers become available, receiver apertures can become smaller.

The use of circularly polarized laser beams may affect discrimination of ambient illumination and thus relieve the narrow-band filter problem.

G. Photomultipliers

Three photomultipliers were evaluated for field research of atmospheric limitations and modulation techniques in optical communications systems.

Type 1 photomultiplier contained 12 multiplier stages and had a 1.68-inch-diameter semi-transparent spherical S-1 photocathode. Measurements at 1500 volts, 25°C, and 8500 Å were:

Sensitivity	2630 μa/μw
Risetime (10 to 90 percent)	2×10^{-9} sec
Anode dark current NEP	5.7×10^{-9} watts

In order to realize the risetime noted above, it was found necessary to cover the tube closely with a shield connected to cathode potential.

Type 2 photomultiplier contained 10 multiplier stages and had a 0.5-inch-diameter semi-transparent S-1 photocathode. This smaller tube was well-suited for liquid nitrogen cooling in the structure sketched in Fig. 11(a). To ensure against seal fracture by thermal shock, the tube was wrapped with tape, the dewar was stuffed with foam rubber, and the liquid nitrogen feed was restricted. A photograph of the cooled photomultiplier assembly is shown in Fig. 11(b). The assembly was designed to mount rigidly to the receiver telescope. Measurements at 1500 volts and 8500 Å were:

	25°C	-196°C
Sensitivity	84 μa/μw	57 μa/μw
Risetime (10 to 90 percent)	1.8×10^{-9} sec	1.8×10^{-9} sec
Anode dark current NEP	1.7×10^{-9} watts	8.7×10^{-11} watts

The improvement in NEP, by a factor of 20, with the liquid nitrogen cooling significantly improved signal-to-noise ratio during nighttime operation. During daytime operation, the NEP

---

*See Appendix A.

was set by the ambient illumination which passed the narrow-band IR filter. In response to large pulse signals, the tube exhibited a fast initial response followed by a larger and much slower response. This behavior suggests a double-valued time constant for the S-1 cathode, which could lead to difficulty in a system encountering a large range of input signals. Gain control by means of intermediate dynode voltages did not affect this behavior.

Type 3 photomultiplier was a developmental model containing 14 stages and an output pulse risetime of 0.5×10^{-9} sec. However, this tube could not be produced successfully with an S-1 photocathode, but it was supplied, for evaluation purposes, with an S-20 photocathode. This photomultiplier was compared with Type 2 for sensitivity at $8500\,\overset{\circ}{A}$ and at 25° and $-196°$C, and was found to be less sensitive by an order of magnitude.

H. AM and FM Electronics

A major factor in the design of the electronics for the field evaluation of AM and FM techniques was the requirement to be able to compare the performance of FM vs AM, essentially, simultaneously. This requirement was imposed by the lack of microthermometric or other means of characterizing atmospheric turbulence. Accordingly, the transmitter and receiver systems shown in block schematic form in Figs. 12 and 13 were developed.

The transmitter electronics consisted of a 28-Mcps oscillator, a power amplifier and DC bias supply which excited a GaAs diode, and means for modulating the RF with both AM and FM on a time-shared basis. An audio signal (980 cps) was switched at a 60-cps rate in order to alternately frequency modulate the RF oscillator and amplitude modulate the plate circuit of the power amplifier. The deviation during the FM period was 5 kcps. The percent of amplitude
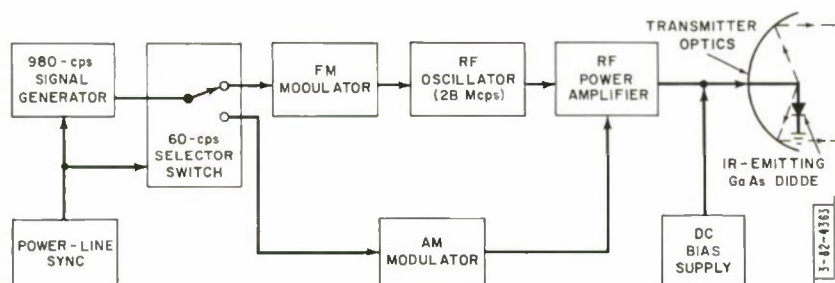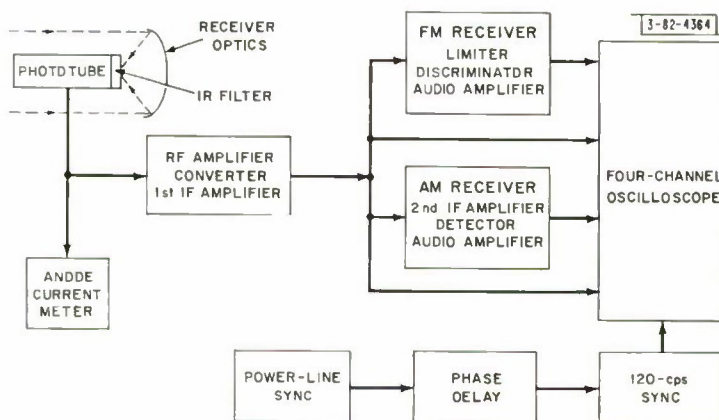

Fig. 12. AM-FM transmitter system.

Fig. 13. AM-FM receiver system.

14

modulation could be controlled through the range of 0 to 100 percent. In this manner, comparisons of the AM and FM techniques could be made without concern about differences in systems factors, viz., excitation power, diode efficiency, optical aperture, beamwidth, pointing accuracy, meteorological condition, receiver aperture and field-of-view, and photomultiplier sensitivity and noise.

The receiver system consisted of a photomultiplier detector, modified AM and FM communications receivers, and a four-channel oscilloscope for signal display. Synchronizing signals for the receiver and transmitter were derived from the power line.

V. FIELD EVALUATIONS OF AM AND FM OPTICAL COMMUNICATIONS

Evaluations of FM and AM optical communications were conducted under a variety of weather conditions during the period from December 1963 through June 1964.

A. Experimental Field System Characteristics

The essential parameters of the system for the comparison of FM and AM optical signals are:

Transmitter

Source	GaAs noncoherent diode
Temperature	$-196°C$
Excitation	Direct current plus 28-Mcps subcarrier Rms current ~ 4 amp
Modulation	
FM	5-kcps deviation, 980-cps audio signal
AM	70-percent modulation, 980-cps audio signal
Wavelength	$8620\,\overset{\circ}{A}$
Radiant power	8 mw (at full aperture)
Beamwidth	$\frac{1}{3}$ to $\frac{1}{2}$ degree
Aperture	Full — 10-inch diameter, variable

Pathlength   1.8 miles

Receiver

Aperture	Full — 10-inch diameter, variable
Field-of-view	$\frac{1}{3}$ to 1 degree
Narrow-band filter	
Center wavelength	$8620\,\overset{\circ}{A}$
Half-bandwidth	$240\,\overset{\circ}{A}$
Center wavelength transmission	60 percent
Detector NEP	
At 25°C	5.7×10^{-9} or 1.7×10^{-9} watts
At $-196°C$	8.7×10^{-11} watts
Noise bandwidth	5 kcps

In choosing the frequency of the RF subcarrier, two considerations were dominant: (1) It was desired to use as low a subcarrier as possible in order to withstand better, without RF
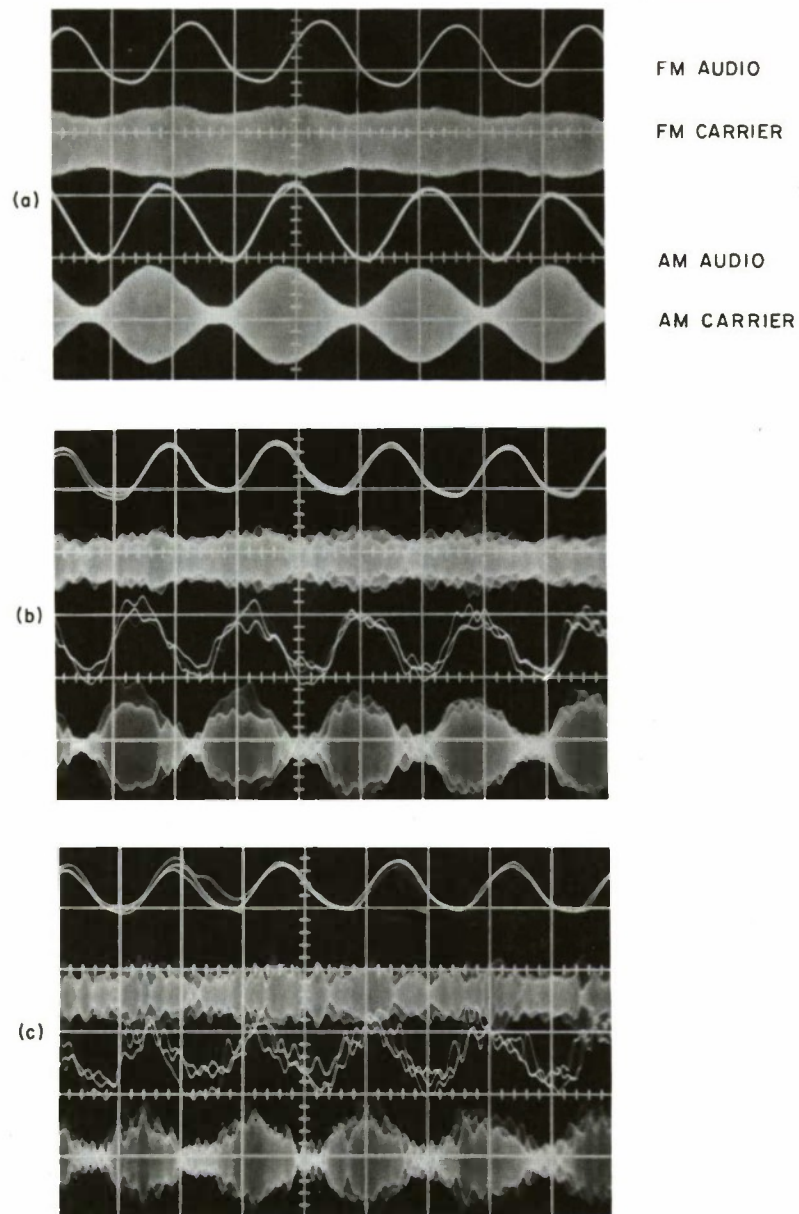
FM AUDIO

FM CARRIER

(a)

AM AUDIO

AM CARRIER

(b)

(c)

Fig. 14. FM and AM optical signals for various transmitter and receiver apertures. Weather: clear path, overcast.

Transmitter	Receiver
(a) full (10-inch diameter)	full (10-inch diameter)
(b) full	small (−17 db)
(c) small (−14 db)	full

carrier "wash out," the transit-time dispersions under poor propagation conditions. (2) It was desired to use a subcarrier frequency whereby audio bandwidth signals could be conveyed using readily available electronic equipment and state-of-the-art techniques. A 28-Mcps subcarrier which permitted the use of inexpensive and readily available commercial transceivers was chosen.

The transmitter employed a variable iris aperture, giving an aperture shape of a circle with a circular occlusion at its center. The receiver employed a rotating shutter aperture, giving partial apertures having the shape of radial segments of a circle. The variable apertures on both the transmitter and receiver optics were calibrated in terms of decibels below full aperture:

$$db = 10 \log \frac{\text{full aperture area}}{\text{partial aperture area}}$$

The optical signals that impinged on the photodetector were attenuated to the same degree as the apertures were stopped down.

The signals displayed by the four-channel receiver oscilloscope were:

(1) The audio signal demodulated from the FM carrier.

(2) The intermediate frequency signal (related to the RF subcarrier) during the FM portion of the cycle.

(3) The audio signal demodulated from the AM carrier.

(4) The intermediate frequency signal during the AM portion of the cycle.

The intermediate frequency signals (2) and (4) are related to the RF subcarrier after detection by the photomultiplier. The IF signals relate the amplitude of the envelope of the RF subcarrier and include noise introduced in the atmospheric path, the photomultiplier tube, and the RF amplifier. For optical signals sufficiently strong compared to the receiver noise, the IF signals give a valid indication of atmospheric scintillation noise. The wide-band receiver noise, in the absence of an optical signal and when passed through the intermediate frequency amplifier (5-kcps bandwidth), takes on narrow-band noise characteristics which are indistinguishable from the multiplicative scintillation noise.

In the series of field data presented in this section (Figs. 14 through 18), the four signals shown on each oscillogram are those described above and are referred to in abbreviated form as:

(1) FM audio

(2) FM carrier

(3) AM audio

(4) AM carrier.

It should be noted that the FM transmitter oscillator was not completely free from amplitude modulation. The degree of this amplitude modulation (about 15 percent) is indicated by the FM carrier trace in Fig. 14(a).

The levels of the four channels were adjusted to obtain good oscillograms; no attempt was made to convey relative amplitude information between different oscillograms. The time scale of the oscillograms is adequately defined by the 980-cps audio signal.
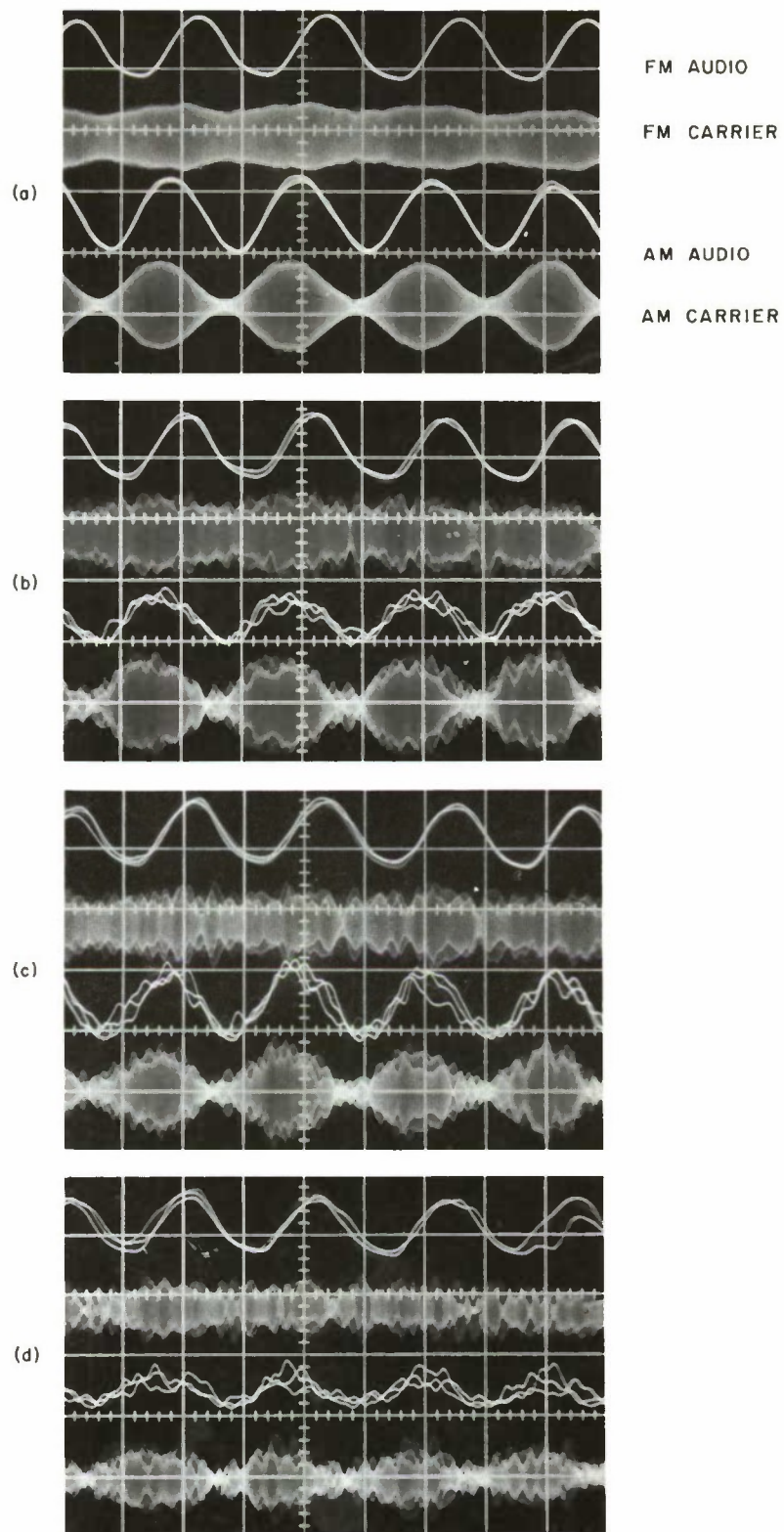
17

Fig. 15. FM and AM optical signals for various receiver apertures. Weather: very hazy, 2- to 3-mile visibility. Aperture: (a) full, (b) −8 db, (c) −17 db, (d) −25 db.

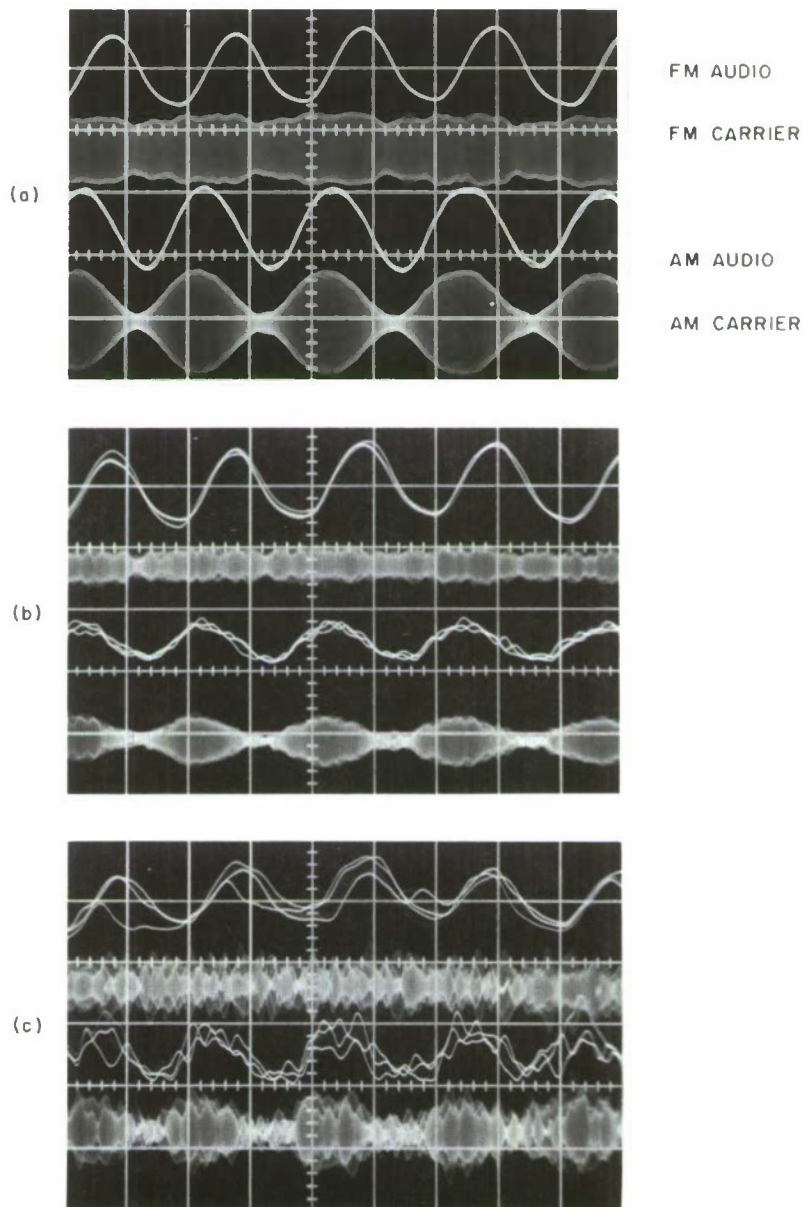FM AUDIO

FM CARRIER

(a)

AM AUDIO

AM CARRIER

(b)

(c)

Fig. 16. FM and AM optical signals through moderate scatter path. Weather: light snow, fog, 31°F, 95-percent relative humidity, 1-mile visibility. Aperture: (a) −3 db, (b) −9 db, (c) −12 db.
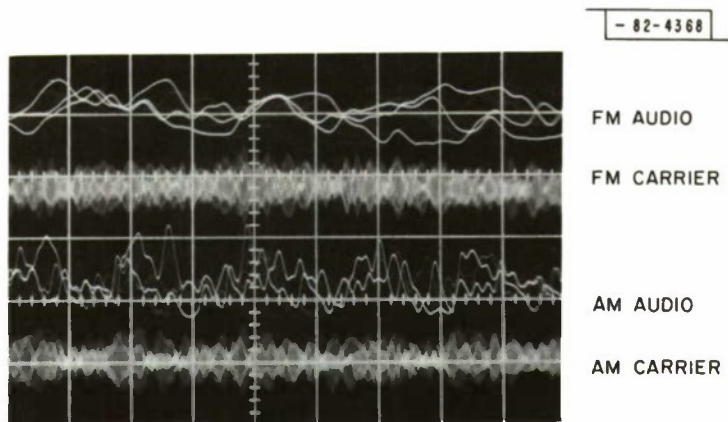
- 82-4368

FM AUDIO

FM CARRIER

AM AUDIO

AM CARRIER

Fig. 17. FM and AM optical signals through heavy scatter path. Weather: heavy snow and fog, less than 0.6-mile visibility.

- 82-4369

FM AUDIO
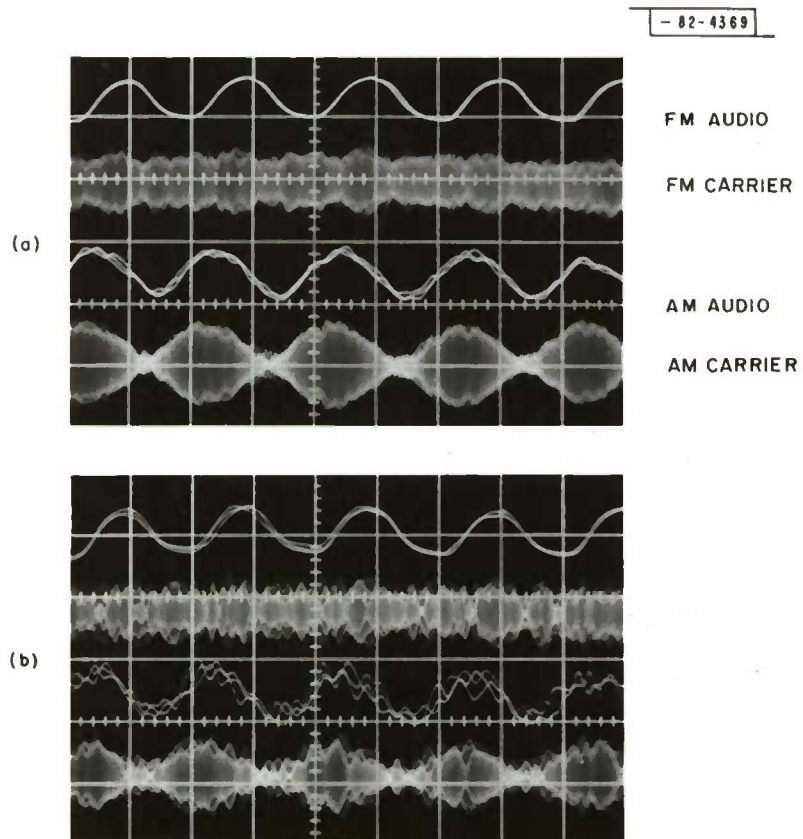
FM CARRIER

(a)

AM AUDIO

AM CARRIER

(b)

Fig. 18. FM and AM optical signals through path with severe visible shimmer. Aperture: (a) −3 db, (b) −9 db.

B. Effects of Path Geometry on Optical Signals

The effects of path geometry as defined by the apertures were apparent from measurements taken under clear-air path conditions, as seen from field data presented in Fig. 14. With full apertures (10-inch diameter) on both transmitter and receiver optics [Fig. 14(a)], only a small amount of scintillation is evident and only on the AM signal. However, when either the receiver aperture or the transmitter aperture is made small [Figs. 14(b) and (c), respectively], the modulation noise on the AM signal becomes quite significant. The optical signals were very much larger than the receiver noise level so that the modulation noise seen in the oscillograms of Fig. 14(a-c) is a true measure of the atmospheric scintillation noise.

The progressive increase in scintillation noise with progressive narrowing of the path geometry by stopping the receiver aperture is shown in the series of oscillograms in Fig. 15(a-d). For the conditions of this test, the optical signal was approaching the receiver noise level; the noise seen in the oscillogram of Fig. 15(d) is largely receiver noise. The effectiveness of the FM technique in overcoming the scintillation is readily apparent in the oscillograms of Figs. 14 and 15.

C. Effects of Weather Conditions on Optical Signals

Scintillation noise occurring in clear-air paths and under hazy conditions, and the effectiveness of overcoming this noise by means of the FM technique, have been demostrated by the tests represented in the oscillograms of Figs. 14 and 15.

The results of tests made during a snow fall accompanied by fog indicate that the signals were attenuated approximately 15 db over the 1.8-mile path when the visibility was 1 mile. Representative oscillograms [Fig. 16(a-c)] show the relative superiority of the FM technique in overcoming the receiver noise which was the dominant source of noise in this test.

Not all weather conditions were penetrable with our available optical signal power. Heavy snow and fog, with visibilities less than $\frac{1}{2}$ mile, generally blotted out the signals completely. Figure 17 shows an oscillogram of a test wherein the 980-cps tone is barely detectable on the FM audio channel. The ear could detect the tone buried in the receiver noise somewhat better than the oscillogram indicates.

Paths through rainfalls were observed to be neither as lossy as paths through snows and fogs, nor as scintillating as many clear-air paths. Paths through clear air with strong winds were more frequently less scintillating than clear-air paths with light winds.

The worst scintillation condition was observed in clear air, with a light breeze immediately following a snowfall approximately one hour after sunset. Severe visible shimmer was evident. Oscillograms of the optical signals are shown in Fig. 18. Scintillation modulations of approximately 25 percent were observed with a receiver aperture of -3 db (equivalent circular aperture of 6.25-inch diameter). Scintillations of approximately 85 percent were evident for a receiver aperture of -9 db (equivalent circular aperture of 3.1-inch diameter). The considerable reduction of noise in the FM channel is evident in the oscillograms. There were occasional bursts of low-frequency components in the scintillation noise that are not evident in the oscillograms. It was impossible to expose clear oscillograms during the brief periods of maximum low-frequency scintillation since the oscilloscope traces would jump. During these periods the AM audio signal as heard by ear contained numerous long "thumps," and the FM audio signal was accompanied by short "clicks."

21

D. Listening Tests on FM and AM Optical Signals

Listening tests were made of speech and music by alternatingly employing FM and AM during periods of pronounced scintillation. The scintillation phenomenon imparts a "mushy" or "garbled" quality on AM transmissions. The quality of FM transmissions was clear. Compared to the AM system, the FM system gives a very noticeable suppression of receiver noise with weak signals; however, there is a rapid degradation in signal-to-noise ratio when signals are reduced below a certain threshold level.

E. Summary of AM and FM Field Evaluation

A summary of the field study of difficult propagation conditions and the relative performance of FM and AM techniques is as follows:

(1) The strong dependency of the degree of scintillation modulation on optics aperture diameter is confirmed. Larger aperture paths incur less scintillation modulation.

(2) Appreciable scintillation has been observed under hazy and clear-air path conditions. The worst scintillation conditions observed on the 1.8-mile path incurred 85-percent modulation for an equivalent circular-aperture diameter of 3 inches.

(3) The FM technique overcomes the scintillation modulation very effectively and permits the use of relatively small apertures.

(4) The FM technique reduces the receiver noise for conditions of weak signals.

(5) The feasibility has been demonstrated of frequency-modulated, 28-Mcps subcarrier, optical communications over a 1.8-mile path through all weather except the heaviest snows and fogs by using the modest radiant power of 8 mw.

VI. INTRODUCTION TO PULSE MODULATION OPTICAL SYSTEMS

The capability of the FM technique in overcoming AM noise occurring in the atmospheric path or in the receiver results simply from the functioning of an FM receiver. The successive stages of amplification and limiting which precede an FM discriminator function to suppress all amplitude variations, essentially leaving pulse rates to be detected. It can be reasoned that PM systems, in which information is extracted by detection of pulse rates, pulse duration or position, or pulse train codes, rather than pulse amplitudes, would be similar to an FM receiver in overcoming AM noise.

A. Advantages of Pulse Modulation

Wide-bandwidth (200 Mcps) communication can be obtained directly with PM techniques which could be achieved with FM techniques only by employing microwave frequencies. As discussed previously, subcarrier frequencies should be as low as possible in order to withstand better the transit-time dispersion incurred by clear-air turbulence or multiple-scatter aerosols.

Wide-band communication is believed to be one of the "natural" applications of semiconductor emitting diodes because of their extremely short time constants. Time constants[10] for GaAs IR emitting diodes are 10^{-9} sec, whereas for GaAs lasers, time constants are limited only by the propagation time through the device, or about 10^{-11} sec. Experimentally, GaAs lasers have been modulated at frequencies up to 11 Gcps.[11]

Another motivation leading to the development of PM communications was the development and availability of semiconductor lasers, with their offer of greatly increased radiant power and high efficiency under high-peak-pulse excitation conditions.

B. Objectives

Our objectives in working with PM optical communications were to:

> Measure the transit-time dispersion of high repetition-rate optical pulses propagated over the 1.8-mile field path for a variety of weather conditions

> Demonstrate the feasibility of a PM system capable of conveying video-bandwidth signals over short ranges with a 98-percent weather operational capability.

Both objectives require the

> Development of semiconductor laser technology in order to attain sufficient signal power.

VII. DEVELOPMENTS IN SEMICONDUCTOR LASER TECHNOLOGY

Developments which were pursued in order to achieve our objectives are presented in this section.

A. Semiconductor Lasers and Arrays

Noncoherent IR emitting diodes were never seriously considered for application in wide-band PM communications systems because of their inadequate radiant power (8 mw at 4-amp peak-pulse drive).

Several GaAs lasers[12] were provided by the Applied Physics Group at Lincoln Laboratory. Microphotographs of one of these lasers are shown in Fig. 19(a-b). The "pill-package" configuration consists of a GaAs laser diode (0.035 × 0.010 × 0.0035 inch) sandwiched between two molybdenum wafers (0.050 diameter × 0.010 inch). Preliminary measurements indicated that 0.5-watt peak, 10-nsec pulses, at a pulse repetition rate of 1 Mpps could be obtained with excitation pulses of 10 amp at 77°K. This laser performance was considered marginal for the objectives previously described.

Although improvements in the efficiency and size of semiconductor lasers are expected as the device technology advances, a factor that limits the amount and applicability of the radiant power is the geometry of a semiconductor laser. In a semiconductor laser the laser activity arises at the junction (see Fig. 20) which is only 5 to 10 microns thick; thus, the active volume is very small, and radiant power from the device is limited. Furthermore, the long, narrow slit shape of the active junction face results in a quite inefficient cross-sectional shape of the projected laser beam. Actually, at the present state of device technology, laser activity occurs only in filaments through the junction volume.

A technique was developed for combining the radiation from multiple lasers with fiber optics so as to produce a laser beam having greater radiant power and an efficient, circular cross section. A bundle of fiber optics is disposed abutting one of the faces of the semiconductor laser such that the entire junction face is covered. During operation, only certain active spots in the junction face emit laser radiation which is conducted by certain fibers in the bundle. These active fibers are selected and combined to form a second substantially smaller bundle, and the inactive fibers in the original bundle are cut off. The cross section of the second active bundle of fibers is of the same order of magnitude as the cross section of the active lasering area of the laser diode junction face. A number of so-constructed laser elements can be stacked in a series
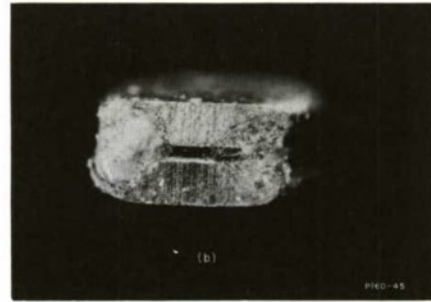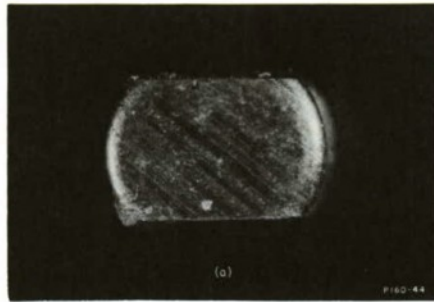
Fig. 19(a-b).   Microphatagraphs af GaAs laser in pill package.
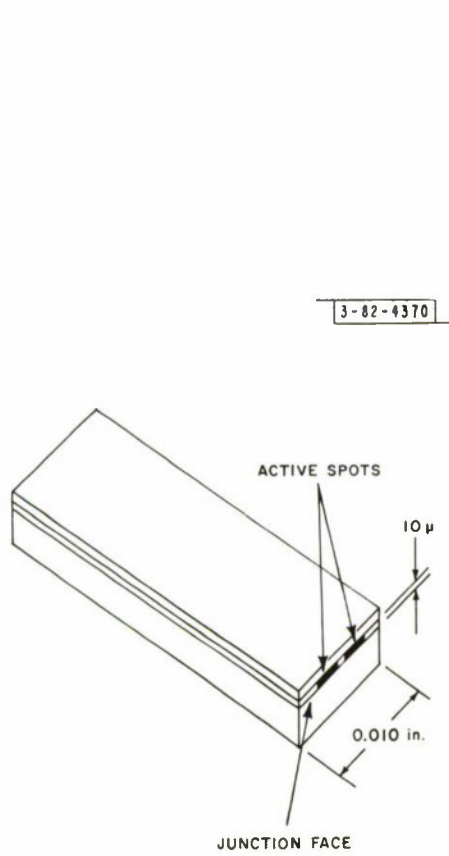
3-82-4370

3-82-4371

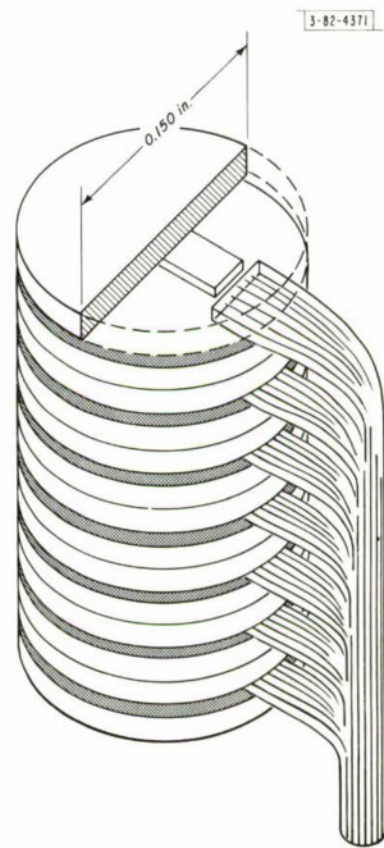Fig. 20.   GaAs laser die.

Fig. 21.   Series array af laser diades.

array as shown in Fig. 21. Since the electrical resistance of each laser is very low (presently 0.1 ohm with potential for further reduction), the number of elements can be excited in electrical series from one pulse generator. The active fiber bundles from each laser element are combined at the focal point of a collimating lens so that a beam of desired cross-sectional shape is projected.

The coherency of the laser radiation is lost in propagating through the many fibers that make up a bundle leading from one laser element, and further, the laser elements of an array are not coherent with each other. However, the property of coherency is of no value per se in the present application, but rather the concurrent properties of spectral purity and high radiance are of value.

At the end of the combined fiber bundles, the radiation leaves each fiber, ideally, at the same angle as was the angle of incidence at the diode end of the fiber. The exit beam will be broadened, however, by anisotropy in the fibers, diffraction effects at the end, lack of end flatness, etc. If the diameter of each fiber is as large or larger than the laser junction width, further broadening of the beam by diffraction at the fiber ends will not be appreciable.

Present GaAs lasers have irregular beamwidths of approximately 10° to 15° resulting from diffraction from the active spots within the laser junction width of approximately 10 microns. If fibers of 10- to 20-micron diameters are employed, the required F-number of the optics system need be no smaller than that required for a laser without a fiber bundle output.

The number of laser elements in array that can be accommodated by an F/5.6 optics system for several specified transmitted beamwidths is calculated as follows.

For present GaAs lasers the junction width is 0.01 inch by approximately 10 microns thick. The active spots may extend along as much as two-thirds of the total junction width giving a total active area of about 1500 microns.^{2} After fabrication of the laser element with a bundle of fiber optics and after cutting off the inactive fibers of that bundle, the remaining smaller bundle of fibers will have an area somewhat larger than the active area of the junction face — about 2000 microns.^{2} The number of these laser elements in array that can be accommodated by an F/5.6 optics system is listed in Table I for several specified optics diameters and transmitted beamwidths.

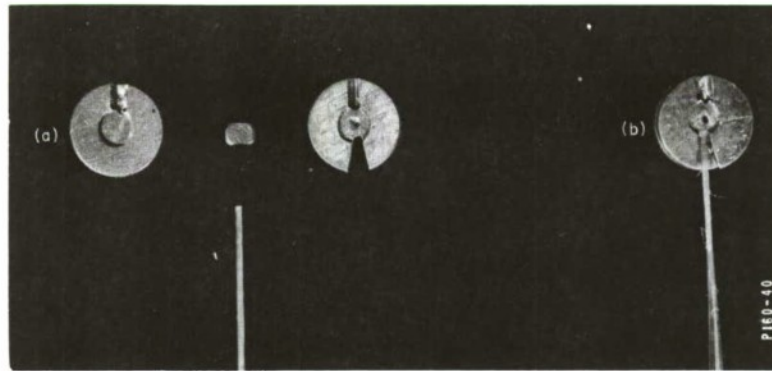| TABLE I				
POSSIBLE NUMBER OF LASER ELEMENTS IN ARRAY				
Beamwidth (mrad)	Primary Optics Diameter (F/5.6 System)			
	2 Inches	6 Inches	10 Inches	48 Inches
0.1	–	3	8	183
0.2	–	11	31	735
0.5	8	71	200	–
2.0	127	1140	–	–

Fig. 22. Model 1 laser element assembly: (a) components before assembly, (b) completed assembly.

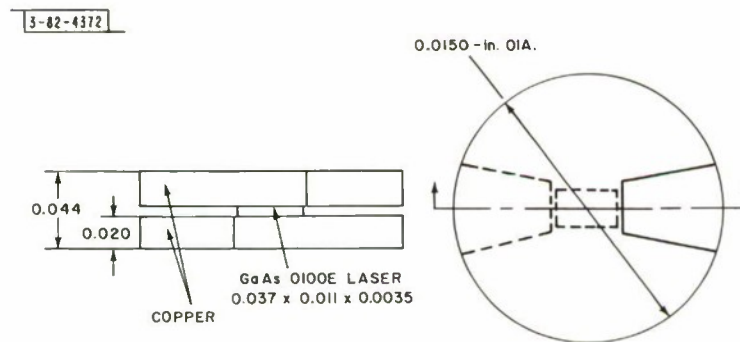Fig. 23. Assembly fixture for Model 1 laser element.

Fig. 24. Model 2 laser pill package.

Transmission efficiency through the short length of fibers (including end losses) is better than 60 percent. The series array structure shown in Fig. 21 is amenable to coaxial feed; the number of laser elements is limited only by the length of the array in relation to the wavelength of the highest driving frequencies and by the ability to dissipate power losses. Liquid nitrogen cooling is required generally.

B. Fabrication of Laser Array Elements

The fabrication of laser elements with fiber optics is given in detail below.

Two models of a laser element assembly, both suitable for series arrays, were developed. Model 1, which consisted of the GaAs die sandwiched between two 0.050 diameter × 0.010 inch molybdenum wafers, employed the laser configuration shown in Fig. 19. Although this configuration was far less amenable to our application than desired, a number of lasers in this configuration were available. Assembly using Model 1 laser elements was successfully accomplished although with difficulty and poor yield. In order to employ these units, it was necessary to sandwich the element, shown in Fig. 19, between two copper wafers (0.150 diameter × 0.020 inch). The copper wafers were recessed to receive the molybdenum pill packages so that a fiber optics bundle could be attached between the copper wafers and also abut the diode junction face. Figure 22 shows a layout of the pieces: two copper wafers, a molybdenum pill package, and a fiber optics bundle. A complete laser element assembly is also shown. The top and bottom of the laser pill package and the recesses in the copper wafers were first wetted with indium. After careful cleaning, these components were stacked in the assembly jig shown in Fig. 23. The loaded assembly jig was heated to 170°C in an argon atmosphere to effect the indium bonding of the components.

The design of the Model 2 laser element is shown in Fig. 24. In this design the GaAs die is bonded directly between suitable copper wafers, and the double sandwich package is unnecessary. GaAs lasers, in this preferred form, were employed as soon as they became available.

The fiber bundles were positioned between the copper wafers and aligned and butted against the GaAs die face with the aid of micromanipulators and a microscope as shown in Fig. 25.

Much experimentation with various epoxy cements proved the suitability of a commercially available bonding agent for attaching the fiber bundle to the copper wafer and withstanding repeated cycling between 25° and −196°C. Detailed technique was critical: 1 gram of agent was mixed with 7 drops of hardener, allowed to set for 1 hour, applied in a thin layer, and cured at 25°C for 1 to 2 days.

After fabrication, the laser element with fiber bundle attached was excited, and the inactive fibers were pruned from the bundle. A sketch of the apparatus used in this process is shown in Fig. 26. The fibers leading from the laser element were fanned out on a stationary platform, and a photodiode with slit aperture was traversed across the fanned out fiber ends. Inactive fibers were broken off by tweezers.

Fibers of 25-micron diameter were obtained from two suppliers. It was necessary, however, to develop the techniques for forming the desired shape of bundle and for bonding, grinding, and polishing the ends. One supplier experienced great difficulty with these techniques and was not able to supply acceptable fiber bundles to specifications. Another supplier suggested a development contract. The techniques which were developed are quite simple, but required much experimentation.

Bundles of forty 25-micron fibers in an orderly 4 × 10 pattern were made in the following manner.
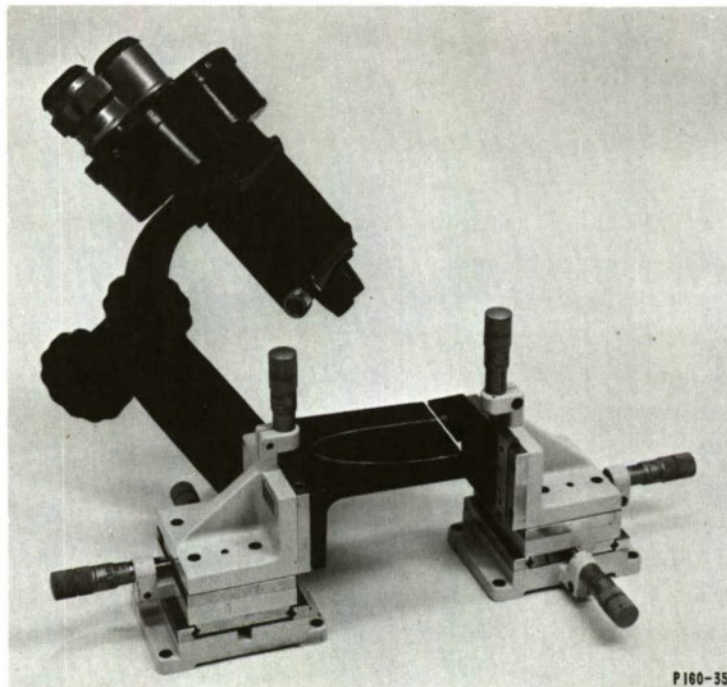
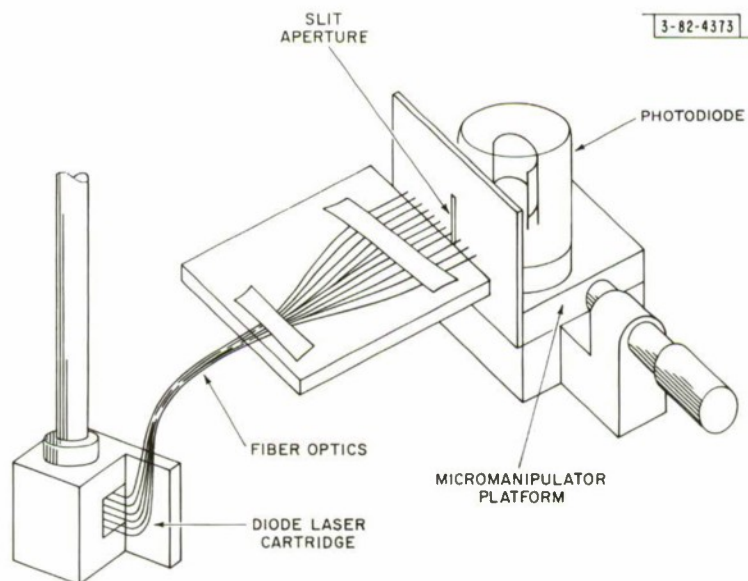Fig. 25. Apparatus for attaching fiber bundle to laser element.

Fig. 26. Apparatus used to select active fibers leading from laser element.

Channel molds were made of three pieces of adhesive-backed teflon tape on a glossy-finish black Bakelite board. The mold, shown in Fig. 27, consists of a bottom tape piece and two top pieces (4 mils thick) separated along their length by exactly 10 mils. Forty fibers (thoroughly cleaned) are laid out evenly in this channel mold by gentle stroking which causes the fibers to adhere to the board by static charge and prevents them from coiling. More tape then secures the fibers. The epoxy bonding agent is applied in very small drops to the top middle of the channeled fibers. Capillary action draws the epoxy down and along the length of the fibers without air inclusions. A dozen bundles can be prepared in this manner by a dexterous person in one hour. After the epoxy is cured, the tape can be peeled off without fracturing the bonded fiber ends.
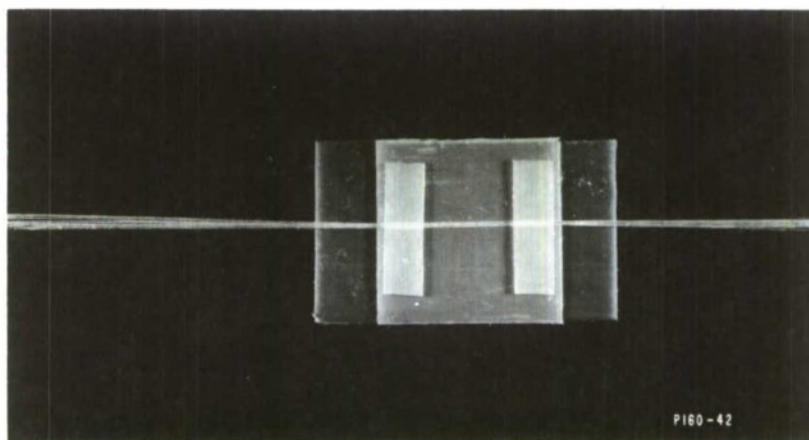

Fig. 27. Fiber optics bundle positioned in teflon tape mold.

The fiber bundle end which abuts the laser and the end of the bundle of selected active fibers must both be ground normal and flat and polished. Both ends are processed in the same manner, but the polishing of the output end requires safety consideration of the laser element already attached to the other end. The end of the bundle, bonded for $\frac{1}{4}$ to $\frac{3}{8}$ inch, is cemented between two pieces of glass, each $\frac{1}{2}$ inch square and $\frac{1}{4}$ inch thick. The glass pieces are heated, a thin coating of resin is applied to one side of each, and then the fiber bundle is sandwiched between the glass pieces and aligned normally. A dozen or more fiber bundles can be processed at the same time. Figure 28 shows a bundle attached to the laser element at one end and cemented between glass pieces at the other end. A specially designed grinding and polishing tool is shown in Fig. 29(a-b). The glass pieces holding the fiber bundles are clamped and sealed in the bottom of the tool; the fiber bundles and laser elements are coiled and taped down inside the waterproof inner chamber. The inner chamber is shaped to avoid bending the fibers beyond their minimum bending radius. Successful grinding has been done by using silicon carbide abrasive powder on a glass plate. Polishing has been done with diamond powder on a polishing lap. After polishing, the fiber bundles are removed from the glass sandwich by heating and then washed in solvent.

A GaAs laser element complete with fiber optics has been cycled between 25° and −196°C over fifty times with no evidence of epoxy failure. It is very necessary, however, that the unit be completely free from moisture before immersion in liquid nitrogen.
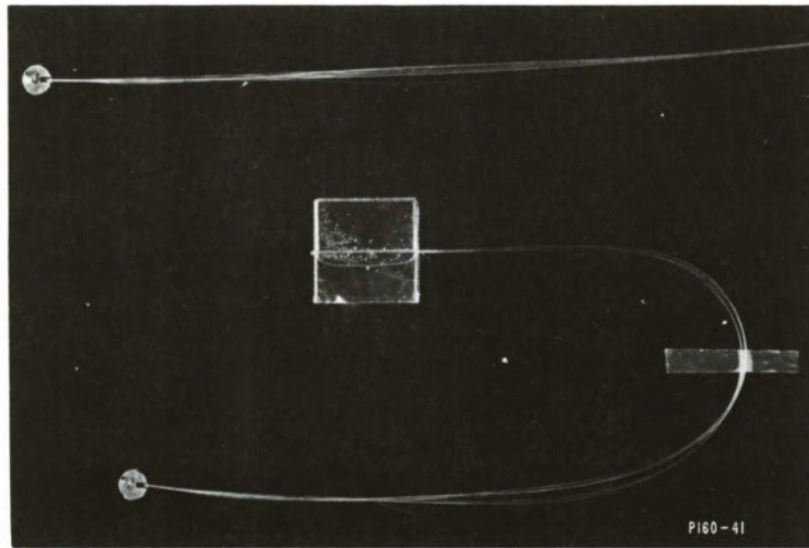
29

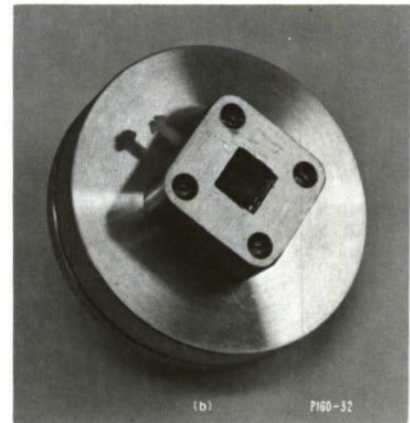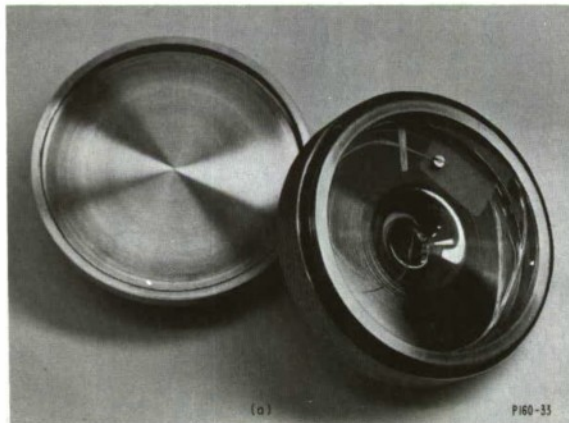Fig. 28.   Model 2 laser element with ottoched fiber optics bundle.

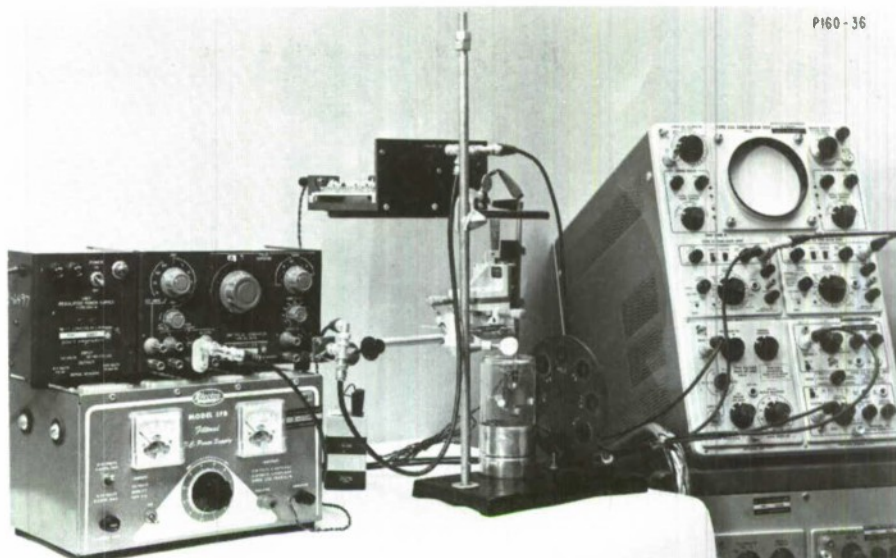Fig. 29(a-b).   Fiber optics grinding and polishing tool.

Fig. 30. Laser measurement apparatus.

C. GaAs Laser Measurements and Evaluation

The GaAs lasers that we evaluated were measured under certain standard test conditions chosen for meaningfulness to PM systems and closely related to standard test procedures employed by the Applied Physics Group who supplied the lasers.

The standard test apparatus shown in Fig. 30 consisted of a pulse generator and pulse current-amplifier, a coaxial cartridge containing the laser, a set of calibrated apertures, a photodiode, and an oscilloscope monitor. Standard driving pulses were 10 μsec wide at a prf of 50 pps and had a controllable peak amplitude from 0 to 25 amp. The lasers were tested under one of two conditions of liquid nitrogen cooling. Under immersion-cooling, the laser radiation was measured through approximately 3/8 inch of bubbling liquid nitrogen. Under "cold-finger cooling," the laser was positioned on a silver electrode which protruded above the liquid nitrogen level by approximately 3/16 inch. The 925 calibrated photodiode operated at 300 volts with a 1-kohm load resistor. Positioned between the laser and the photodiode were a set of apertures (F/1.4 through F/11) contained in a wheel which could be rotated to snap into precision alignment any one of the calibrated apertures. An F/1.4 aperture was specified for standard test conditions. The laser cartridge was mounted on an X-Y micropositioner which was used to optimize alignment before the test measurements.

Radiant power measurements under standard test conditions and cold-finger cooling are given in Table II for a number of GaAs lasers. All the lasers radiated from two sides of the GaAs die; no reflective coatings were employed on either junction face. Generally, the lasers were measured within a day of delivery and repeat measurements were made at various intervals on some units. Between measurements, the lasers were exposed in an air-conditioned laboratory. A number of changes in measurements were observed. Experience with early units indicated that if the drive pulse exceeded a certain value, a sudden and irreversible decrease in output would occur. Accordingly, current drive pulses were limited to 15-amp peak. Some units showed an unexplainable decrease in radiant power with time, whereas others showed a significant increase.

TABLE II

GALLIUM ARSENIDE LASER MEASUREMENTS

Unit	Notes	Side	Threshold Current (amp)	10-Amp Pulses		15-Amp Pulses	
				Radiant Power (mw)	Quantum Efficiency (percent)	Radiant Power	Quantum Efficiency (percent)
405	At time of delivery (unit changed at 20 amp)	A	5.2	610	8.2	1.5 w	13
	After change	A	5.8	570		1.0 w	
414	At time of delivery	A	5.6	300	3.9	650 mw	5.8
600	At time of delivery	A	6.0	170	2.3	440 mw	3.9
	One month later	A	6.5	170	2.3	570 mw	5.0
	One month later	B	6.5	370	4.9	1.0 w	8.9
601	At time of delivery	A	9.0	50		350 mw	3.1
602	At time of delivery	A	6.5	110		350 mw	3.1
	Three days later	A	7.5	80		310 mw	
	One day later	A	>15	7		15 mw	
603	At time of delivery	A	3.5	610	8.1	1.1 w	9.8
	One month later after much use	A	3.5	580		1.0 w	
415	Before assembly	A	5.5	260	3.5	610 mw	5.4
	Before assembly	B	5.5	235	3.1	435 mw	3.9
	After assembly and measured through fibers	A	4.5	260		650 mw	
	After assembly	B	4.5	305		610 mw	

Radiant power output under standard test conditions with 15-amp current drive pulses ranged from 0.35- to 1.5-watt peak from one side. Quantum efficiency, computed as two times the radiant power from one side divided by the volt-amperage across the laser junction, increased with higher drives and ranged from 3 to 13 percent at current drives of 15 amp. Unit 415 improved in power output following assembly in the Model 1 configuration with a fiber bundle. The improvement was evident from both sides of the unit and is believed to have resulted from some beneficial effect of heating in inert atmosphere during the assembly process. In fact, a number of instances of power output instability suggest surface contamination of the junction face, such as might produce a partial electrical short across the junction or change the reflectivity and thus the optical cavity Q. Slight changes in thermal conductivity through the contact between the pill package and the silver electrode could cause changes in junction temperature and thus power output. However, every effort was made to minimize differences in contact pressure by the design of the cartridge which is described in a subsequent section.

Generally, the Model 2 laser elements were tested while immersed in liquid nitrogen. The bubbling nitrogen imparted a modulation on the radiant power, and the peak readings taken by different operators were found to be different by factors of two or three. Standard test pulse waveforms are shown in Fig. 31(a-c). It was found that the radiant pulse amplitude fluttered with a recurrent peak every 1 or 2 seconds; an occasional peak having an amplitude twice the recurrent peak amplitude occurred once every 20 or 30 seconds. The recurrent peak values were accepted as valid. One possible explanation for the higher occasional peak values is that at that instant, nitrogen gas bubbles cover both junction faces, increasing the internal reflectance and improving the optical cavity Q, which results in a brief peak in conversion efficiency.

The occasional higher peak outputs diminished with each cycle of liquid nitrogen immersion, measurement, return to room temperature, exposure to laboratory atmosphere for 1 to 2 days, repeat immersion, etc. A very thin coating of epoxy on the junction faces eliminated these higher peak outputs without measurable change in the recurrent peak outputs.

Figure 32 shows the radiant power characteristics of a Model 2 laser element before and after the fiber bundle attachment. When measured through the fiber bundle, the power output
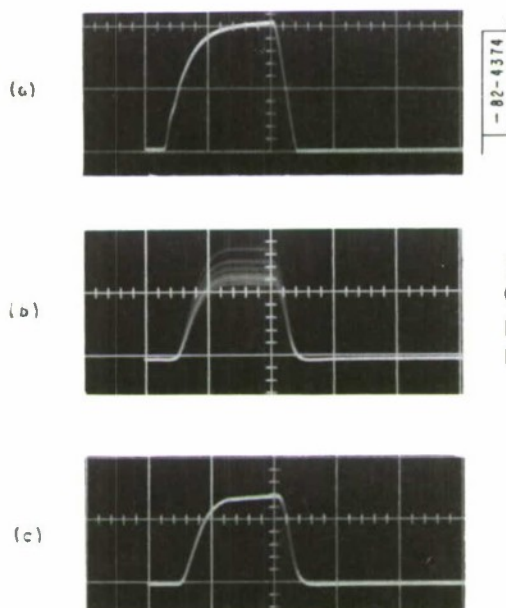

Fig. 31. Standard laser-test waveforms: (a) excitation pulse 5 amp/cm, (b) laser pulse through liquid nitrogen, (c) laser pulse through fiber optics bundle.
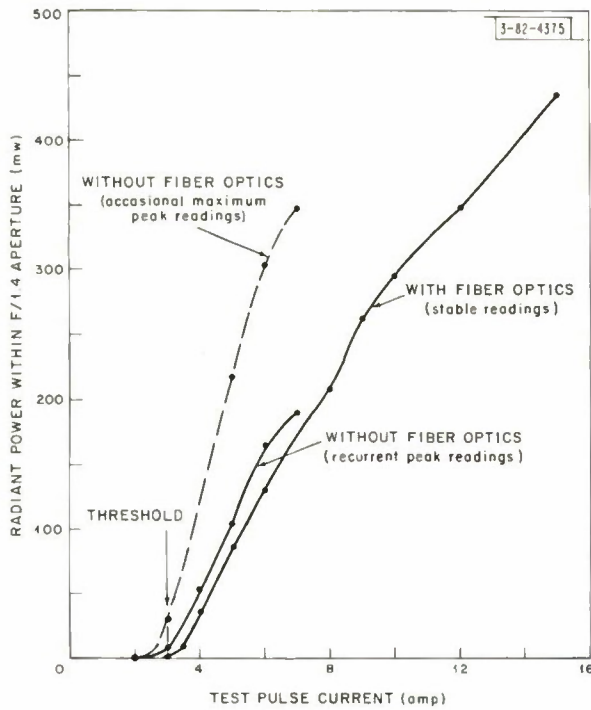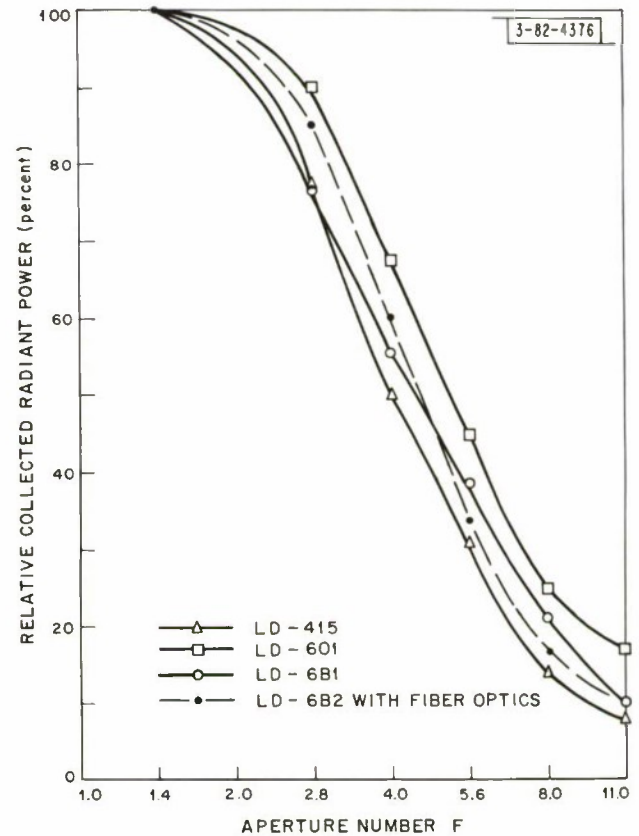
Fig. 32. Radiant power characteristics of a GaAs laser (unit LD-682) totally immersed in liquid nitrogen. Standard test conditions: pulse width = 10 μsec, prf = 50 pps.

Fig. 33. Beamwidth characteristics of GaAs lasers.

was completely stable. The loss through the 6-inch fiber bundle was of the same order as the loss through the $\frac{3}{8}$ inch of liquid nitrogen. Beamwidth characteristics are shown in Fig. 33 for several laser elements, including one emitting through a 6-inch fiber bundle. In this characteristic, the radiant powers contained within the various apertures are normalized to the power within the F/1.4 aperture. The broad beamwidth of these particular semiconductor lasers dictates the use of low F-number optics. Beam broadening by the fiber bundles (25-micron-diameter fibers) is insignificant.

A series array was successfully fabricated using a room-temperature-setting epoxy solder to cement the laser elements together. The total radiant power from the array of two elements was the sum, within measurement accuracy, of the radiant powers from each element excited separately.

D. Pulse Generators

Pulse generator requirements were set by the objective of demonstrating the feasibility of a PM system capable of conveying video-bandwidth signals. After consideration of pulse rate, pulse code, pulse width, and pulse-position modulation (PPM) schemes, the PPM appeared to be most efficient in terms of attainable bandwidth and peak-pulse power for an allowable power dissipation within the laser. A PPM system was envisioned in which the video signal is sampled at twice the highest video frequency or 10 Mcps. Pulses are as narrow as technology permits, about 10 nsec, and the pulse positions are modulated in accordance with the signal sample amplitudes (see Appendix B).

The PPM scheme, therefore, sets the following objectives for pulse generator performance.

Amenability to modulation
Pulse width = 10 nsec
Prf = 10 Mpps.

Current drive for the GaAs lasers, required a

Pulse peak current = 10 amp, minimum

and the pulse generator would be required to drive a number of laser elements (1 to 15) that were stacked in series array or

Load impedances = 0.1 to 1.5 ohms.

The objective of measuring transit-time dispersion required of the generator:

Fastest possible pulse risetimes
Minimum pulse-leading-edge jitter.

A number of components and techniques were considered for the pulse generator application. These included dry and mercury-wetted reed switches, four-layer semiconductor devices, avalanche transistors, spark gaps, thyratrons, Krytrons, power transistors, and vacuum tubes. Some sophisticated techniques using multiple avalanche transistors looked attractive but involved an unpredictable amount of development effort and risk. Since pulse generator technology was rather far-afield of our objectives, it was decided to pursue the more predictable approach, albeit "brute force," of vacuum tubes.

An E-H Research Laboratory Model 120-D pulse generator served as a primary source. The unit can be used either as a periodic pulse generator driven by its own internal source with
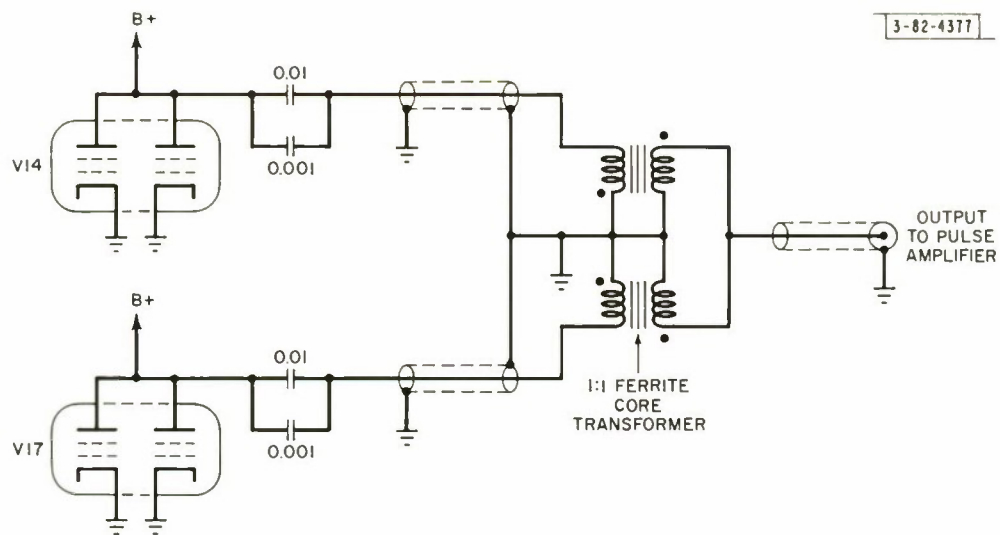
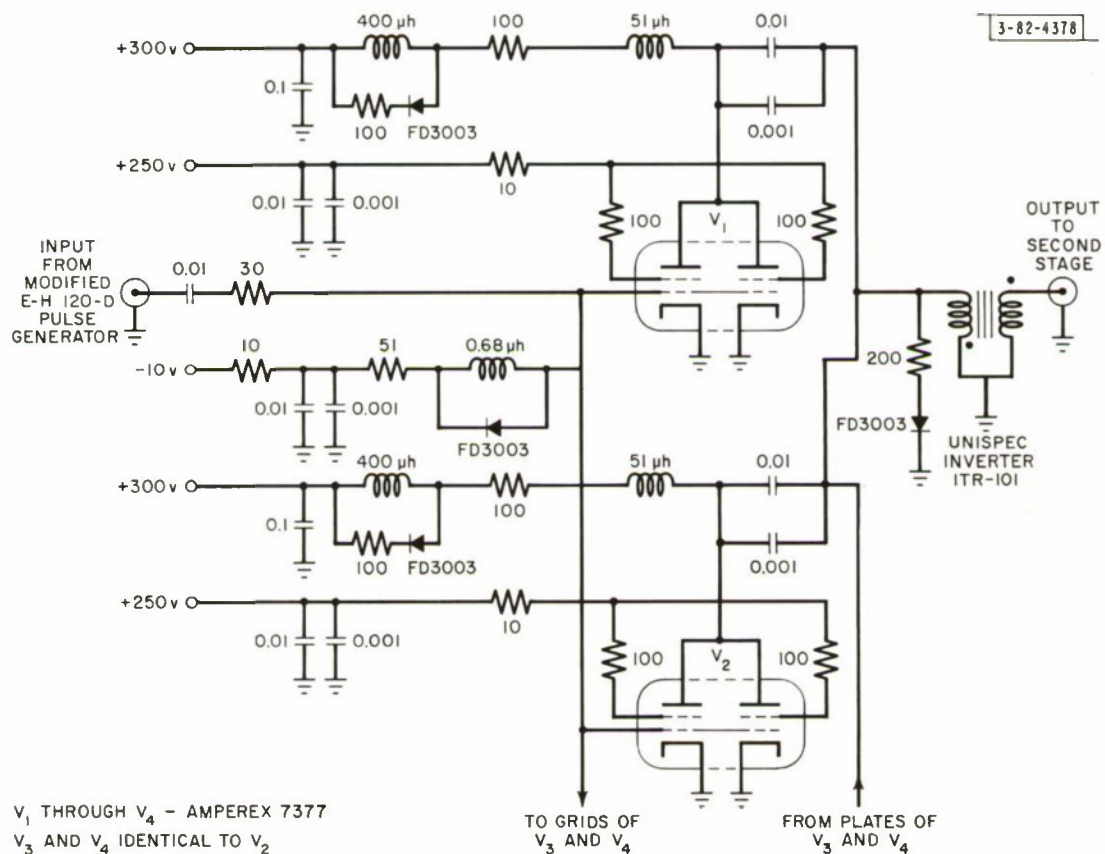Fig. 34. Modificotian of E-H 120-D pulse generator.

V_1 THROUGH V_4 – AMPEREX 7377
V_3 AND V_4 IDENTICAL TO V_2

Fig. 35. First stoge of pulse omplifier.

36

prf's above 10 Mpps or as a pulse amplifier driven by an external and modulated pulse source. The 120-D provides two outputs of 10-nsec 25-volt pulses into 50 ohms, with risetimes of 1.0 to 1.5 nsec. The instrument was modified, according to the schematic shown in Fig. 34, to obtain a single output of 50-volt pulses into 50 ohms. Attempts were made to transform the output pulses to give 10-amp pulses into a 1-ohm load. Included in the transformer designs was a distributed line transformer, produced on order by E-H. Transformer losses were high, resulting in 4-amp pulses into a very short 1-ohm strip line. Matching laser diodes to the strip line and maintaining liquid nitrogen cooling was not successful.

A two-stage pulse amplifier was developed to follow the 120-D pulse generator. Schematics of this pulse amplifier are given in Figs. 35 and 36. The first stage consisted of four 7377 tubes in parallel, and the second stage consisted of eight 7377 tubes in parallel.

A high-current transformer was developed to couple the output of the 8-tube final amplifier to a 1-ohm coaxial line.

A sketch of the pulse transformer is shown in Fig. 37. The transformer employs a single Q-2 toroid core, eight bifilar-wound primaries, and a single-turn secondary formed by the enclosing brass case. The coaxial line is connected to the transformer through ten 10-ohm resistors in parallel, which serve as a 1-ohm monitoring resistor while also reducing multiple reflections from the diode laser load which is generally mismatched to the line.

The layout of the amplifiers was very critical, requiring great attention to attain short lead lengths and symmetry among the tubes of each stage. Figure 38 shows a photograph of the second-stage amplifier construction.

A 1-ohm coaxial line design was employed which was concurrently developed on another program.* Stainless steel rods, of 0.250-inch diameter were coated with 0.004-inch thickness of Durafilm — a teflon-base insulator with a dielectric constant of 3.67. This process was performed by American Durafilm Company, Inc., Newton Lower Falls, Massachusetts. The coated rods were chemically copper flashed and then copper electroplated to an outer conductor thickness of 0.025 inch.

The performance of the vacuum-tube pulse amplifier is indicated by the oscillograms of output pulse waveforms shown in Fig. 39(a-d). Peak pulse currents above 10 amp were obtained for prf's to 6 Mpps. The pulse amplitude decrease at high prf's resulted from power supply limitations and increasing problems of clipping-diode saturation. Pulse widths, measured halfway between laser threshold current (3.5 amp) and peak current, were 10 nsec. The post pulse ringing is of no consequence because it is below laser threshold. The current pulse waveforms above threshold were not significantly affected by loads ranging in impedance from 0.1 to 1.5 ohms

E. Laser Cartridge Development

A coaxial cartridge was developed to accommodate the several laser element designs: the pill-package design (Fig. 19), the Model 1 and Model 2 assemblies with fiber bundles (Figs. 22 and 24), and series arrays of the laser elements (Fig. 21). The laser cartridge is shown in a cross-section drawing in Fig. 40 and in an expanded layout in Fig. 41. The inner conductor of a coaxial line (A) screws into a cartridge electrode (D) which is machined from a section of 1-ohm coaxial line and soldered into position. Electrical contact is made to the laser element or array

*The 1-ohm coaxial line was developed by J.D. Welch, Group 42, Lincoln Laboratory, on a program under contract NAS9-105.

Fig. 36. Second stage of pulse amplifier.
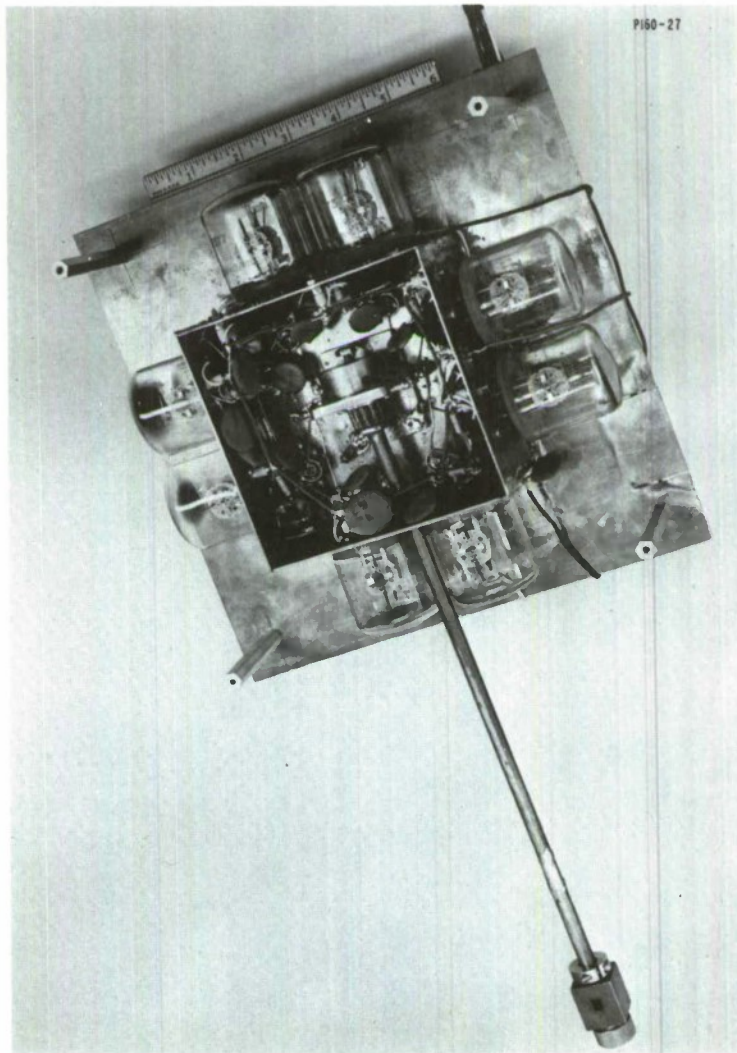

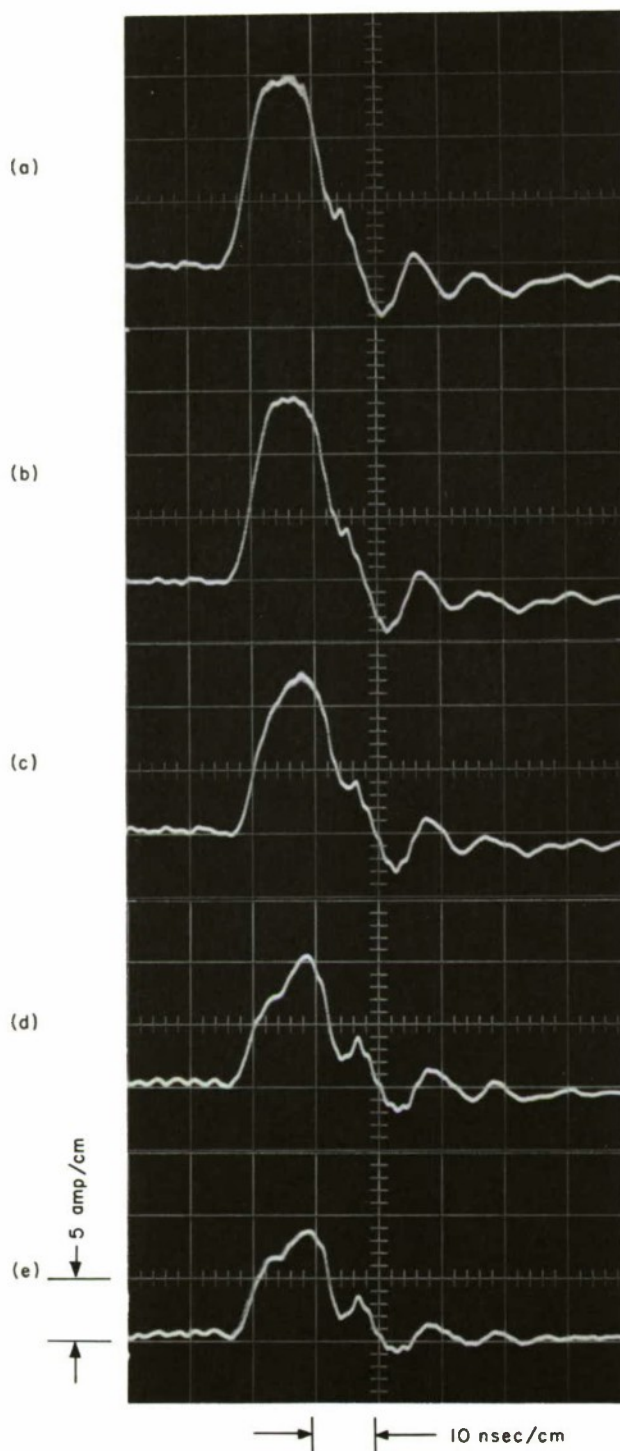Fig. 37. High-current pulse transformer.

Fig. 38. Pulse amplifier.

Fig. 39. Pulse amplifier waveforms. Prf: (a) 200 kpps, (b) 1 Mpps, (c) 2 Mpps, (d) 5 Mpps, (e) 10 Mpps.
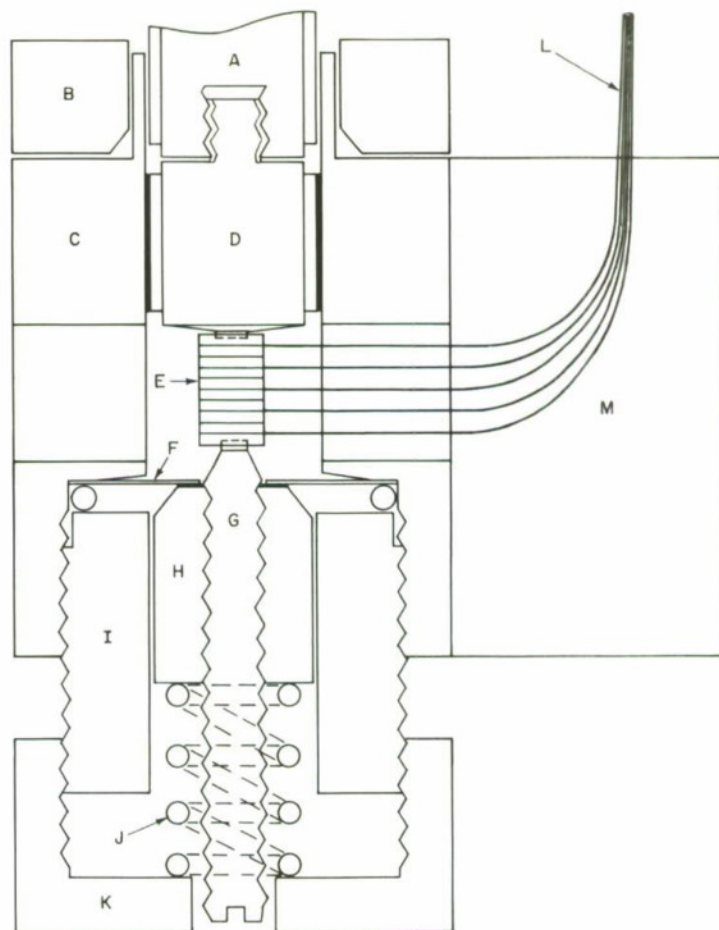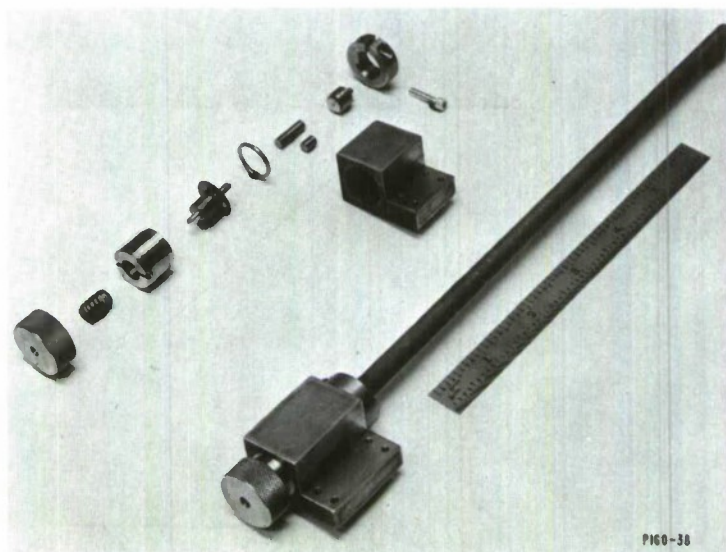
Fig. 40. Laser cartridge.

Fig. 41. Exploded view of laser cartridge.

41

by advancing a screw electrode (G) until a very light mechanical contact is made. Then the cap (K) is tightened, compressing a spring (J) and exerting a force on a piston (H) which glides in a cylinder (I) and is restrained by a diaphragm (F). The difference between the compression force of the spring (J) and the deflection force of the diaphragm (F) is transmitted without a rotational shearing component to the contacts between the laser element and electrodes (G) and (D). Previous cartridge designs employed an electrode which rotated while advancing against the laser element; laser elements were frequently fractured by shear forces. The opposing forces of the spring and the diaphragm permit precise and repeatedly accurate control of contact pressure. The current pulse passes through the laser element or array, the silver electrode (G), the copper piston (H), the copper diaphragm (F), the copper cartridge body (C), and through the pressure contact between the cartridge body and the outer conductor of the coaxial line resulting from tightening the split-collet (B). This electrical path permits the passage of 10-nsec pulses, which contain ultra-high frequency components, without appreciable distortion caused by reactive impedances.

The cartridge has windows on opposite sides to accommodate lasers which radiate from both junction faces. A shoulder (M) is provided on one side for securing the fiber bundles (L).

Two models of cartridges were fabricated, differing only in body length. The shorter cartridge accommodates a laser array composed of up to 5 elements, whereas the longer cartridge accommodates arrays of 13 elements.

Figure 42 shows the shorter model of the laser cartridge, which contains two laser elements of the Model 2 design in series. The active fibers of each bundle have been selected and combined.

Fig. 42. Cartridge containing laser array with fiber optics.

In certain low-duty-cycle applications, the thickness of the copper wafers of the Model 2 laser element (Fig. 24) can be reduced, thus permitting more elements in one cartridge. The cartridges were designed with rectangular cross sections to facilitate close packing of multiple cartridges.

VIII. FIELD RESEARCH ON PULSE-MODULATION OPTICAL COMMUNICATIONS

The PM optical communications system was evaluated under a variety of weather conditions during January 1965.

A. Experimental Field System

A block schematic of the experimental PM system is shown in Fig. 43. The transmitter consisted of the pulse generator and pulse amplifier (described in Sec. VII-D) which excited a single cooled GaAs laser element. The transmitter optics consisted of a $2\frac{1}{4}$-inch-diameter F/1.0 double-convex lens. Figure 44 shows a photograph of the transmitter system.

The receiver system, shown in Fig. 6, consisted of a Type 1 photomultiplier mounted in a 10-inch-diameter telescope and followed by a sampling oscilloscope. A wide-band chain amplifier could be employed to obtain signal levels compatible with pulse circuitry.

System performance characteristics were measured in the laboratory. Figure 45(a-e) shows the waveforms of the laser pulses as measured by the receiver system. In this set of performance data, the current drive pulse was maintained at 5-amp peak as the prf was changed from 1 to 11 Mpps. The 10- to 90-percent risetime of the laser pulses is 4.5 nsec and the half-power pulse width is 10 nsec. Figure 45 includes an oscillogram of the current drive pulses at a prf of 11 Mpps. It is seen that the post pulse ringing on the drive current does not excite the laser which has a threshold current of 3.0 amp.

The decrease in laser pulse power with increasing prf is attributed to the heating of the laser junction. Figure 46 gives output characteristics for a Model 2 laser element for two conditions of cooling and two levels of current pulse drive. Under the condition of cold-finger cooling [curve (A)], laser pulse power decreases rapidly above 2 Mpps. The use of the laser element assembly with fiber bundle output permits the laser to be totally immersed in liquid nitrogen without incurring modulations caused by nitrogen bubbles. Cooling by immersion is far more effective than cold-finger cooling. Useful pulse powers are obtainable at prf's up to 11 Mpps. Higher current pulse drives (at high prf's) have two opposing effects: (1) an increase in laser efficiency by overcoming laser losses (see Table I), and (2) a decrease in efficiency resulting from junction temperature rise. A net gain in efficiency was realized by employing higher current pulse drives at the higher prf's as seen from curves (B) and (C) of Fig. 46. Unfortunately, pulse amplifier limitations did not permit employing 10-amp pulses at higher than 6 Mpps. The 100-percent peak radiant power for curve (C) of Fig. 46 corresponds to 300 mw.

Laser system wavelength characteristics are shown in Fig. 47(a-b) for both cold-finger cooling and for immersion cooling of a laser element with fiber optics. It is seen that the immersion cooling permitted by the fiber optics affords a vast improvement in wavelength stability. The half-power waveband was 65 Å and quite independent of current drive and prf's. The wavelength stability of the immersed laser elements was sufficiently good to permit the use of 1-percent narrow-band filters in a receiver system. The performance of the PM optical system was evaluated in operation across a 20-foot path in the laboratory. For this evaluation
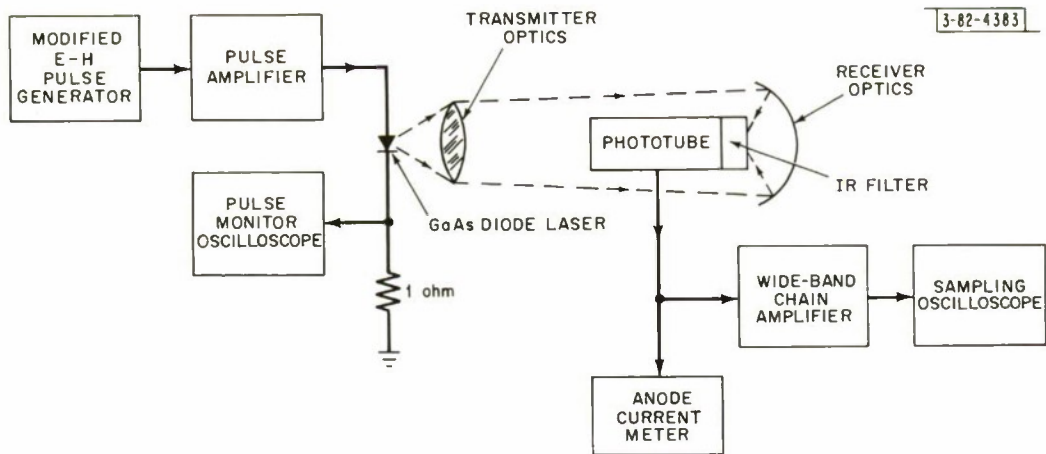
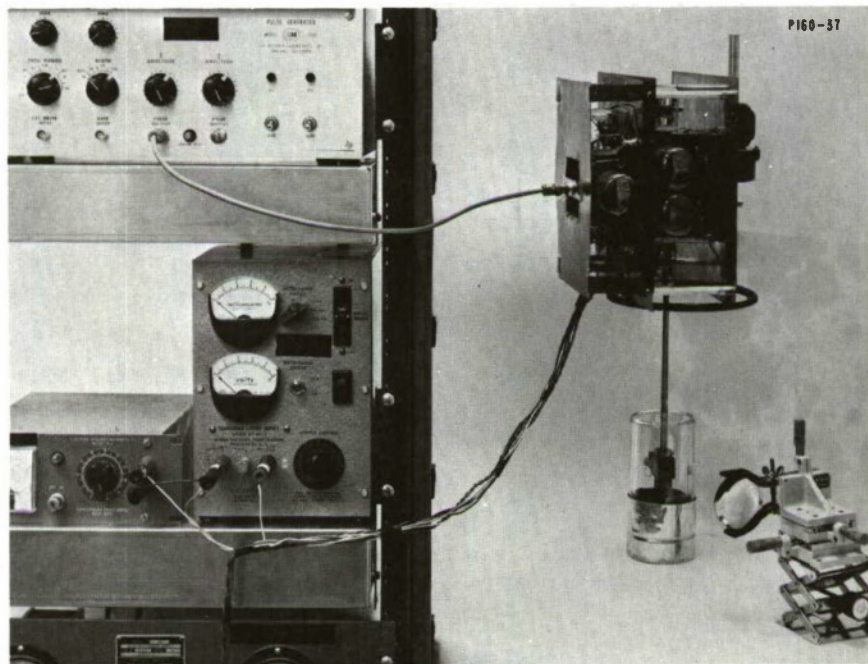43

Fig. 43. PM optical communications system.

Fig. 44. PM optical transmitter system.
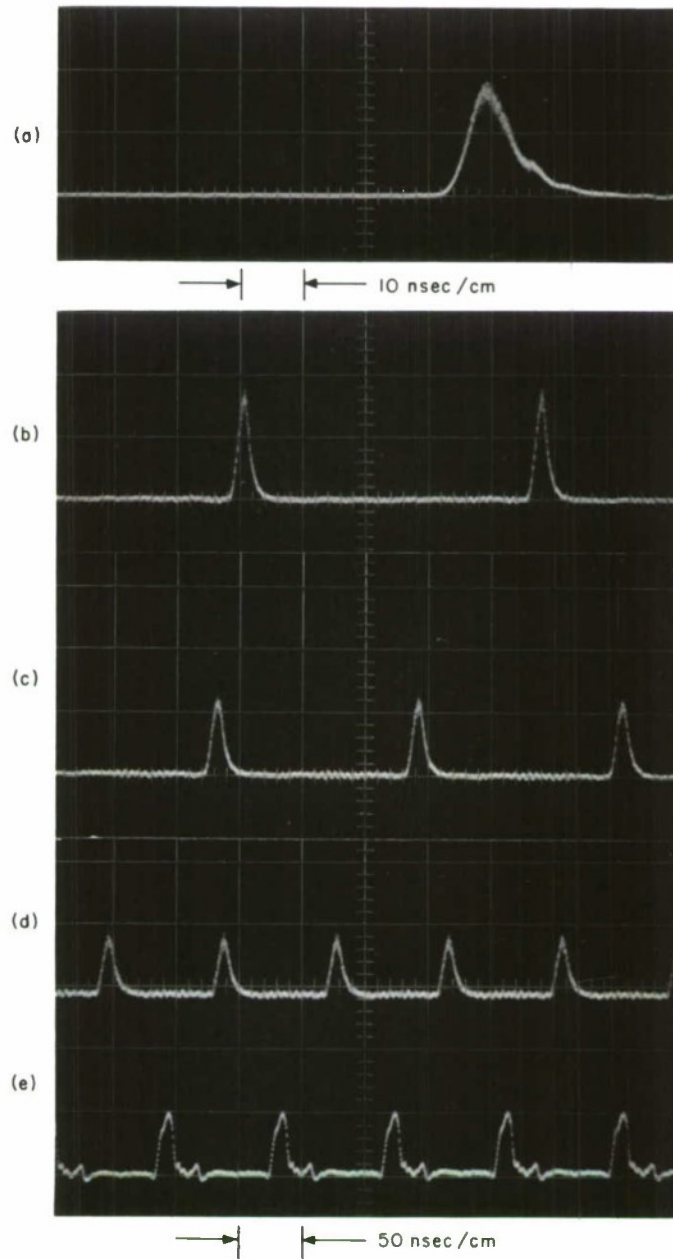
(a)

10 nsec /cm

(b)

(c)

(d)

(e)

50 nsec /cm

Fig. 45. Laser pulse system waveforms. Prf: (a) 1 Mpps, (b) 4 Mpps, (c) 6 Mpps, (d) 11 Mpps. Current drive pulse (e) 11 Mpps.
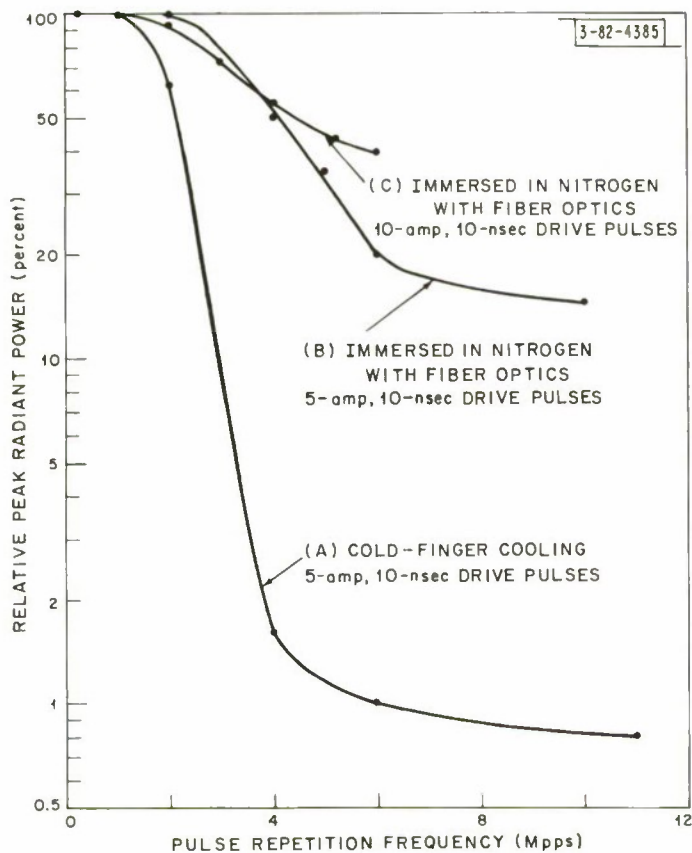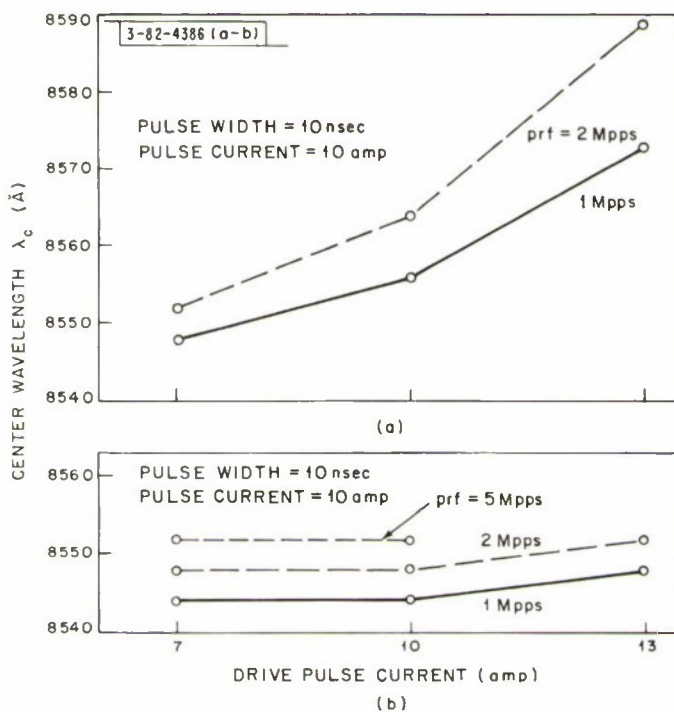
45

Fig. 46. Laser radiant power characteristics.

Fig. 47. Laser wavelength characteristics: (a) laser element with cold-finger cooling, (b) laser element with fiber optics immersed in liquid nitrogen.

no receiver collecting optics were needed, and optical attenuator filters were inserted in the path to yield threshold signal levels. The response of the receiver system to threshold signal levels under laboratory path conditions is shown in Fig. 48. The oscillograms, recorded by 1/25-second camera exposures of a sampling oscilloscope display, show typical receiver response to threshold signals for a range of prf's from 1 to 2 Mpps, current drive pulses of 5 to 10 amp, and photomultiplier voltage of 1400 to 1600 volts. It is against these responses that reception under field conditions will be compared.

As noted previously, the attainment of sufficient signal power for the pursuit of our objectives was the most critical problem. The unavailability, at the time, of a sufficient number of good laser elements restricted the field experiments to the use of a single laser element rather than a stacked array of lasers. Attention was directed toward improving the receiver system sensitivity. It was found that the chief limitation of the receiver system was the high signal-to-receiver noise ratio required for stable synchronization of the sampling oscilloscope. The use of a separate channel to convey a clean sync signal from the transmitter to the sampling oscilloscope would provide 10 dh more signal sensitivity. An attempt was made to provide a sync signal channel by radio communications for the field experiments. However, a sufficiently wide and clean channel could not be found throughout the HF and VHF radio spectrum. A microwave link was considered too costly. The field tests were performed, therefore, to the extent possible with the limited available signal power.

The following lists the essential parameters of the PM optical system used in the field tests.

Transmitter

Source	One GaAs laser (Lincoln Laboratory)
Temperature	$-196°C$
Excitation pulses	10-nsec width, 10- to 15-amp peak
Prf	1 to 2 Mpps
Wavelength	8550 Å
Radiant peak power	300 to 435 mw
Beamwidth	1 degree
Aperture	$2\frac{1}{4}$-inch diameter

Pathlength   1.8 miles

Receiver

Aperture	10-inch diameter
Field-of-view	$\frac{1}{3}$ degree
Narrow-band filter	
Center wavelength	8548 Å
Half-bandwidth	240 Å
Center wavelength transmission	60 percent
Detector NEP	5.7×10^{-9} watts
Noise bandwidth	200 Mcps

B. Field Measurements with PM Optical System

The first set of field measurements employing the PM optical system was taken during clear, cool weather with a light breeze. The time of day chosen was one hour after sunset, in order
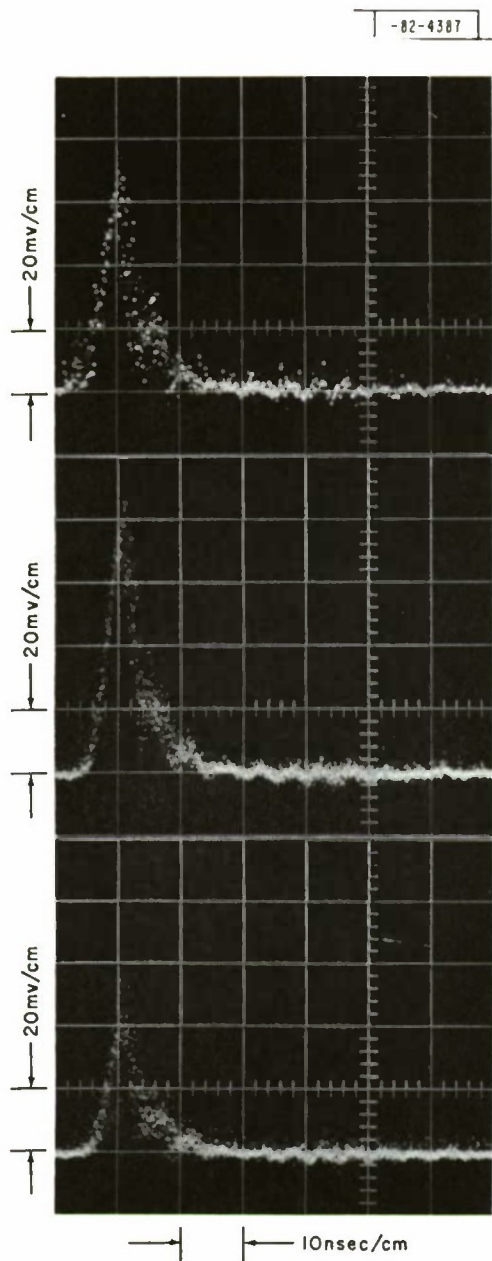
Fig. 48. Threshold signals received over short laboratory path.
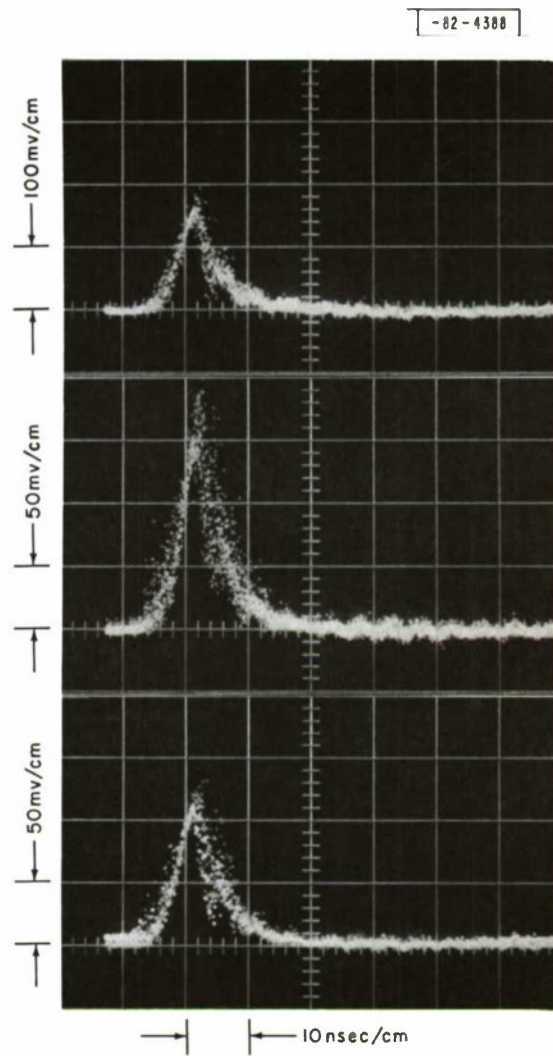

Fig. 49. Signals propagated through clear-air path with light breeze.

to avoid high ambient illuminations. Oscillograms of typical signals received during this test are shown in Fig. 49. Comparison of these signals with the threshold signals received under laboratory conditions (Fig. 48) indicates no appreciable deterioration in risetime or leading-edge dispersion.

A second set of field measurements was taken during overcast and humid, but clear, weather with winds of 15 to 25 mph. The time of day was approximately two hours after sunset. Figure 50(a-c) shows oscillograms of signals on this test. The signal was first recorded with close-to-maximum receiver gain [Fig. 50(a)] and then measured with sufficient optical attenuation (12 db) at the receiver to yield threshold signals [Fig. 50(b)]. Insertion of 14-db optical attenuation reduced the signal below the level required for stable synchronization of the oscilloscope [Fig. 50(c)]. Thereby, it was determined that the system had a signal-to-threshold-signal ratio of approximately 13 db under clear-air path conditions. Again, no appreciable deterioration of risetime or leading-edge dispersion is indicated. The post pulse ringing which is noted on some oscillograms occurs in the photomultiplier tube at its highest operating voltage and is not representative of the received optical signal.

The third and final field test was conducted during weather conditions of snow, sleet, and fog at temperatures of 29° to 30°F, a relative humidity of 100 percent, and winds of 15 to 25 mph. During the period from 6 to 8 p.m., the visibility repeatedly ranged from less than 0.3 mile to more than 2.0 miles. Oscillograms of the received pulses are shown in Fig. 51(a-e). Some small dispersion of the leading edge and degradation of risetime becomes evident for conditions of visibility less than 1.1 miles. For visibility conditions of less than 0.6 mile, the 13 db of signal strength above threshold level was lost in the atmospheric path and signals could not be measured.

The risetimes and the leading-edge dispersions have been carefully measured from the original photographs which are reproduced in Figs. 48 through 51. The risetimes were measured between 10- and 90-percent amplitude points and midway in the sampling trace width. The leading-edge dispersions were measured (see Table III) as the widest trace width above the 30-mv level, chosen as being approximately $\frac{1}{2}$ the peak level of threshold signals.

Since the transmitted pulses were not ideal but had a finite risetime (5 nsec), the channel risetimes are somewhat less than the risetimes of the received pulses. If the pulse shape and the channel response were exponential functions, then

$$\tau_c = \sqrt{\tau_t^2 - \tau_r^2}$$

where

$\tau_c \equiv$ channel risetime

$\tau_t \equiv$ transmitted pulse risetime

$\tau_r \equiv$ received pulse risetime.

For the worst visibility condition for which a threshold signal was measured over the 1.8-mile path, the relation above yields

$$\tau_c = 5 \text{ nsec}$$

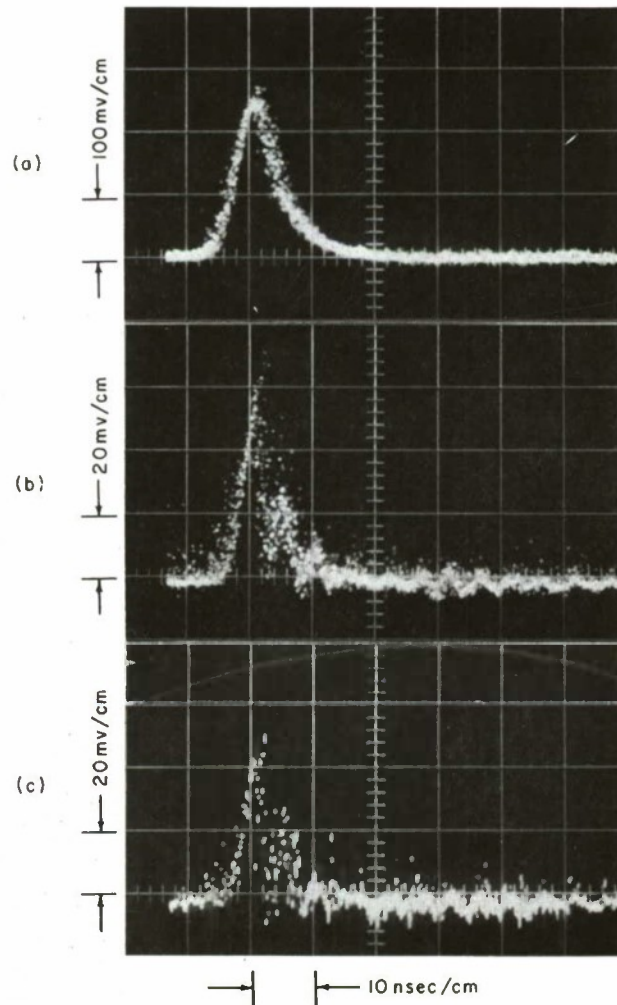or a channel bandwidth of the order of 200 Mcps.

Fig. 50. Signals propagated through clear-air path with winds: (a) na optical attenuatar inserted, (b) 12-db aptical attenuatar inserted, (c) 14-db aptical attenuatar inserted.
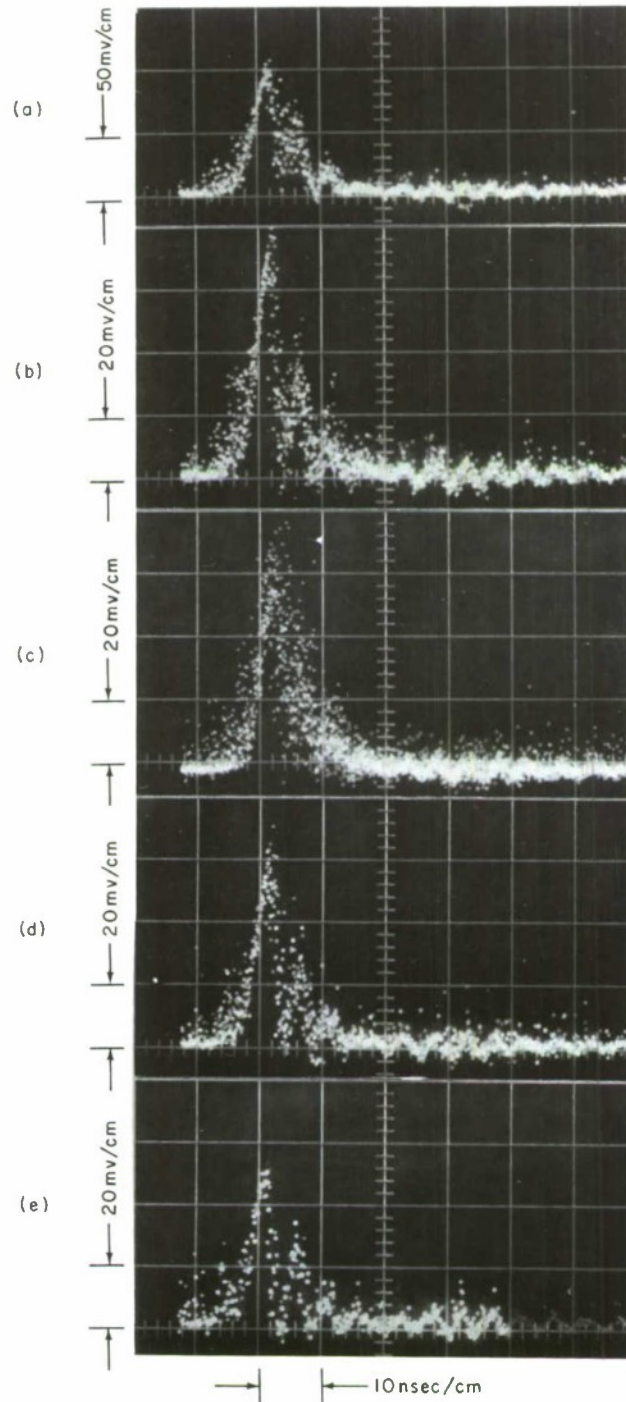
Fig. 51. Signols propagoted through snow, sleet, and fog. Visibility:
(o) 1.1 miles, (b-d) 0.6 to 1.1 miles, (e) 0.3 to 0.6 mile.

TABLE III			
MEASUREMENTS OF PROPAGATED OPTICAL PULSES			
Test Conditions	Figure No.	Risetimes (nsec)	Leading-Edge Dispersion (nsec)
Short loboratory path	48	5	1.5 to 3
Clear, light breeze	49	5.5 to 6	2.5 to 3.5
Clear, windy	50	5 to 6	2.5 to 3
Snow, fog; visibility $\geq$ 1.1 miles	51(a)	5 +	4 +
Snow, fog; visibility −0.6 to 1.1 miles	51(b-d)	6 to 7	4.5 to 5.5

Inspection of the oscillograms of Figs. 48 through 51 reveals a significant variation of pulse peak amplitudes which can be attributed to amplitude modulations imparted by the atmospheric path. Since the transmitted pulses had a 5-nsec risetime, the amplitude modulations would also contribute to the observed leading-edge dispersion. It is possible that this effect could account for as much as $\frac{1}{3}$ of the measured leading-edge dispersion, depending of course on the response of the sampling oscilloscope to such signal amplitude fluctuations.

It may be concluded that fluctuations in the atmospheric path transit-time characteristics are less than the difference between transmitted and received leading-edge dispersions, and less than 4 nsec for the worst visibility conditions for which a threshold signal was measured over the 1.8-mile path.

C. Summary of PM Optical System Field Evaluation

A summary of the field evaluation of the PM optical system is as follows:

(1) Optical pulses propagated over a 1.8-mile clear-air path, with still or windy air, incur no appreciable deterioration of risetime or leading-edge dispersion.

(2) Propagation through the atmosphere, particularly under heavy scatter conditions, imparts an amplitude modulation on the optical pulses. Under the worst conditions measured and for the particular system used in the measurements, the amplitude modulations could incur a leading-edge jitter no greater than 2 nsec. Thus, the PM technique effectively overcomes the limitations incurred by atmospheric path amplitude modulations.

(3) Pulses propagated through a 1.8-mile path under conditions of snow, sleet, fog, and limited visibility incur some deterioration. For the worst visibility conditions measured (visibility of 0.6 mile), the channel bandwidth was of the order of 200 Mcps.

(4) The feasibility has been demonstrated of wide-band PM (10-nsec pulses at prf of 2 Mpps) optical communications, over a 1.8-mile path through all weather except the heaviest snow and fog, using a single GaAs laser element having a peak radiant power of 435 mw.

IX. CONCLUSIONS

In the first half of this report, the general superiority of FM over AM optical communications was indicated. The FM subcarrier technique was shown to permit use of smaller optical apertures, to overcome scintillation modulations occurring in the atmospheric path, and to reduce receiver noise for conditions of weak signals.

In the latter half of this report, the measured transit-time dispersions of high repetition-rate optical pulses propagated over a 1.8-mile path for a variety of weather conditions was presented. For the worst propagation conditions (visibility of 0.6 mile), channel bandwidths of the order of 200 Mcps are indicated. An analysis of laser communications through multiple-scattering paths is presented in Appendix A.

The feasibility of a PM system capable of conveying video-bandwidth signals over short ranges with a 98-percent weather operational capability requires either a single laser device having appreciably higher radiant power than present devices, or an array of multiple laser elements. The technology of series array of multiple laser elements has been successfully developed as indicated by laboratory tests on simple arrays. A number of applications of this new technology are discussed in Appendix B.

APPENDIX A
LASER COMMUNICATIONS THROUGH MULTIPLE-SCATTER PATHS

Although the theory of electromagnetic scattering is directly applicable to many practical problems involving single-scatter phenomenon, application of rigorous theory to multiple-scatter situations leads quickly to mathematically unwieldy equations. Computers may be used to advantage to solve certain of these complicated formalizations. The approach taken here is essentially a ray-tracing analysis of very limited scope, made possible by great simplifications and assumptions. The rough answers obtained with the aid of a simple desk calculator are believed to be pertinent to practical and immediate questions on the subject of laser communications through multiple-scatter paths.

Consider an incoherent, monochromatic, ideally collimated beam having radiant flux P (watts) at a cross section, distance r from an origin where the initial radiant flux is P_o (Ref.13). A unit thickness of the medium will absorb and scatter out of the beam a power proportional to P,

$$dP = -\sigma P dr$$

which integrates to

$$P = P_o \epsilon^{-\sigma r} \tag{A-1}$$

where σ = extinction coefficient $[m^{-1}]$. This function may be interpreted as the distance, in terms of σr, to which various fractions of the incident beam penetrate before being scattered or absorbed. The mean of the pathlengths that incremental fractions of the incident beam penetrate is

$$\ell \equiv \bar{r} \simeq \frac{1}{\sigma} \quad . \tag{A-2}$$

This distance is called the optical thickness or the "mean path."

The volume scatter function,[13] expressed in radiometric terms, is

$$\beta(\varphi) = \frac{J(\varphi)}{H_o v} \tag{A-3}$$

where $J(\varphi)$ is the radiant intensity (watts/steradian) which is scattered at an angle φ from the incident collimated beam of irradiance H_o (watts/m^2), and $\beta(\varphi)$ has the dimensions of m^{-1} The volume scattering function is defined or measured for a volume v of dimensions sufficiently small that multiple scattering does not occur therein and that all emanations may be considered as arising at a central point within the volume.

For our multiple-scatter path analysis, it is necessary to proceed with a mean path volume scatter function

$$\beta_\ell(\varphi) = \frac{J(\varphi)}{H_o a \cdot \ell} = \frac{J(\varphi)}{P_o \ell} \tag{A-4}$$

defined for an elemental volume of length ℓ and having relatively much smaller cross dimensions of area a. It is assumed here that the multiple scattering that occurs within a mean path does not appreciably alter the volume scattering function; thus,
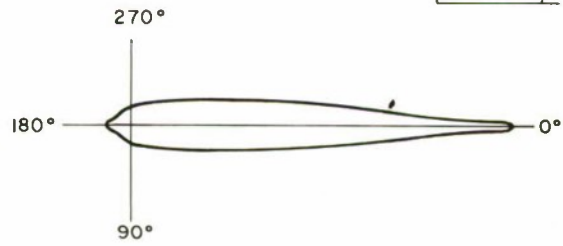
$$\beta_\ell(\varphi) \simeq \beta(\varphi) \tag{A-5}$$

270°

180° ———— 0°

90°

Fig. A-1.   Volume scattering function β(φ) for clouds and fog.

270°

180° ←———————→ 0°

α

90°

Fig. A-2.   Abstracted volume scattering function.

180° ———————————→ 0°

P_0 P_s α P_s P

Fig. A-3.   Model of mean path volume scattering element, $\ell\beta_\ell(\phi)$.

We now abstract the essential characteristics of $\beta_\ell(\varphi)$ such that simple computations will reveal the propagation properties of paths much longer than ℓ. Figure A-1 depicts the $\beta(\varphi)$ function assumed for conditions of clouds and fog having particles large compared to the wavelength, wherein forward scatter is dominant.[14,15] Our attention is restricted here to these conditions. The essential features of the $\beta(\varphi)$ function are maintained if it is reduced to two dimensions and abstracted by vectors representing forward scatter at small angle α and vectors representing side- and back-scatter components (see Fig. A-2). The mean path volume scatter function $\beta_\ell(\varphi)$ will be equal to this abstracted volume scatter function within the approximation of the assumptions noted above.

By abstractly representing the volume scatter function by collimated emanations at discrete scatter angles rather than emanations divergent through a continuum of scatter angles, the radiant intensities $J(\varphi)$ defining $\beta_\ell(\varphi)$ become radiant fluxes $P(\varphi)$. Our further use of the abstracted mean path volume function will involve interception of and accountability of all the forward-scattered radiant flux by ray tracing, so that we need not be concerned, at this point, with having dropped the divergence feature in the definition of $\beta_\ell(\varphi)$.

Rewriting Eq. (A-4) with $P(\varphi)$ replacing $J(\varphi)$, we obtain

$$P(\varphi) = P_o \ell \beta_\ell(\varphi) \quad . \tag{A-6}$$

Phenomenological values for the elemental volume of length ℓ are chosen as follows: From Eqs. (A-1) and (A-2), at the distance ℓ,

$$P(\varphi = 0) \sim 0.4 \, P_o \tag{A-7}$$

which is the "direct beam" penetrating the elemental volume without loss or scatter.

To characterize a dirty, absorptive, cloud or fog condition, the remaining radiant flux $0.6 \, P_o$ is apportioned, somewhat arbitrarily, between the total scattered flux P_s and the absorbed flux P_a:

$$P_s = 0.45 \, P_o$$

$$P_a = 0.15 \, P_o \tag{A-8}$$

Since the side- and back-scattered components total an order of magnitude less than the forward-scattered components, as shown in Fig. A-2, and since these components go off in directions of no interest, we lump the side- and back-scatter components with the absorbed component:

$$P_s(\text{forward}) = 0.4 \, P_o$$

$$P_a + P_s \text{ (side and back)} = 0.2 \, P_o \tag{A-9}$$

The final abstracted model representing the mean path volume scatter element appears in Fig. A-3, wherein,

$$P(\varphi = 0) = 0.4 \, P_o$$

$$P(\varphi = +\alpha) = 0.2 \, P_o$$

$$P(\varphi = -\alpha) = 0.2 \, P_o \tag{A-10}$$

We next set up an atmospheric path model that consists of an ordered array of elemental mean path volumes into which an incoherent, monochromatic, ideally collimated beam impinges
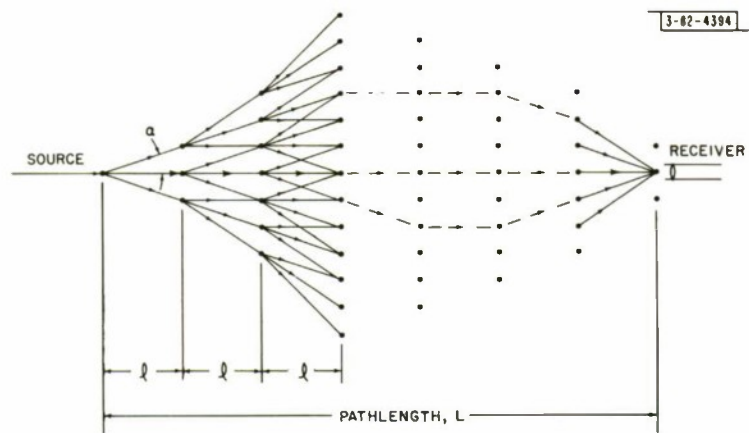
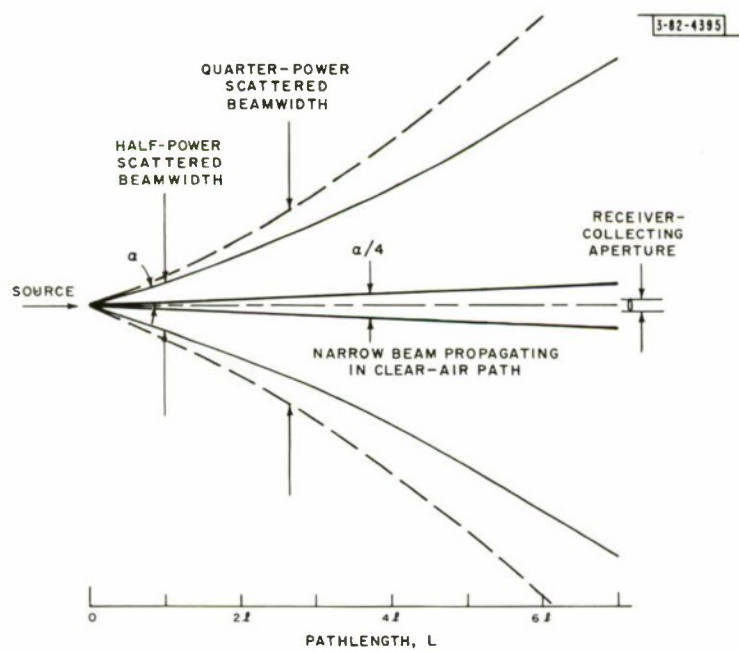Fig. A-4. Multiple-scatter path model.

Fig. A-5. Scattered and clear-path beamwidths.

as shown in Fig. A-4. Each elemental volume passes and scatters incident flux according to the mean path volume scatter model represented in Fig. A-3. Each successive mean path layer of elemental volumes intercepts all the direct and scattered flux emanating from the preceding layer of elemental volumes – which justifies Eq. (A-6). Simple, but tedious, calculations have been made to trace the flow of incident flux through the model for a distance of seven mean paths. Figure A-4 traces the total of the rays for three mean paths and a few typical multipaths for seven mean paths.

At each point in the matrix of elemental volumes, the incident flux has been calculated. From these values the half-power and quarter-power beamwidths at each successive mean path distance have been derived as shown in Fig. A-5. The beamwidths are drawn as continuous curves and to the same scale as Fig. A-4. Note that the half-power beamwidth progressively increases beyond 2α for longer pathlengths. Had we chosen a smaller absorption coefficient and a scattering coefficient compensatingly greater than the values reflected in Eq. (A-8), we would find that the scattered beamwidth would diverge more rapidly than for the chosen case. Also, the scattered beamwidth would diverge a little more rapidly had we included side-scatter components in the analysis.

In view of the large scattered beamwidth, it is seen that we were overstrict when formulating the path model in specifying that the source was ideally collimated. A nominally narrow beamwidth source, for example, having a beamwidth of $\alpha/4$, would result in a slightly increased scattered beamwidth over the values shown in Fig. A-5, with a consequential decrease in incident flux at each point within the beamwidth. However, the greatest error in calculated flux at any point throughout the path, derived on the basis of the ideally collimated source model, would be less than 10 percent. Figure A-5 includes a representation of a beam of narrow width $\alpha/4$ propagating under clear-air conditions and impinging on a receiver collecting aperture. The exact shape of the beamwidth under clear-air path conditions, whether we are considering a beam in its Fresnel or Fraunhofer region, is not important in comparison with the much larger scattered beamwidth. Thus, we can see that under multiple-scatter conditions, there is little advantage in employing a very-well-collimated source such as may be obtained with gas and solid lasers. A nominally narrow source, such that its beamwidth is of the order of $\alpha/4$ or smaller, results in practically the same scattered beamwidth and flux density. Beamwidths of the order of a fraction of a degree such as are readily obtained with semiconductor laser sources are quite adequate.

Calculations have been made of the flux impinging on a collecting aperture of fixed area, a, positioned at successive integer mean pathlengths along the optical axis. These data are shown in Fig. A-6 as continuous curves representing (1) the total signal flux received by a wide-angle field-of-view optics system, and (2) the direct beam signal flux which experiences no scatter.

It is seen that most of the signal flux received by a wide-angle collector at a distance of four mean paths or greater consists of flux which has been scattered. It seems intuitive that our path model would be equally applicable to a coherent source as to the presumed incoherent source. Although intense variations of radiant flux over very small dimensions, within the beam at short path lengths, could be expected to result from wave phase coherence, these effects would be washed out rather quickly by the myriad random locations and motions of the scatter particles.
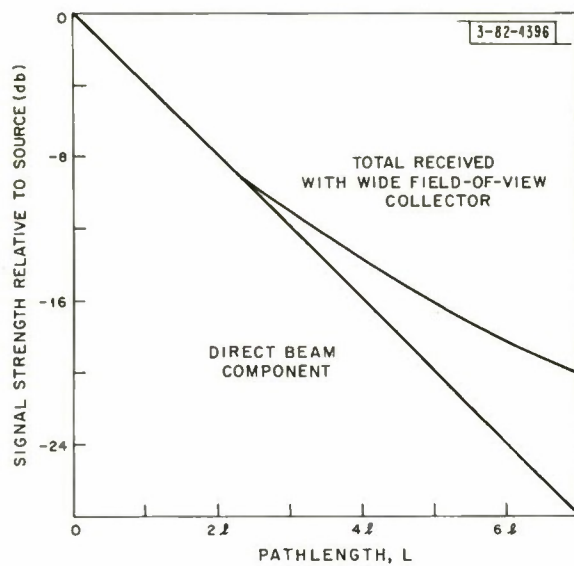
Fig. A-6. Signal vs pathlength characteristics.

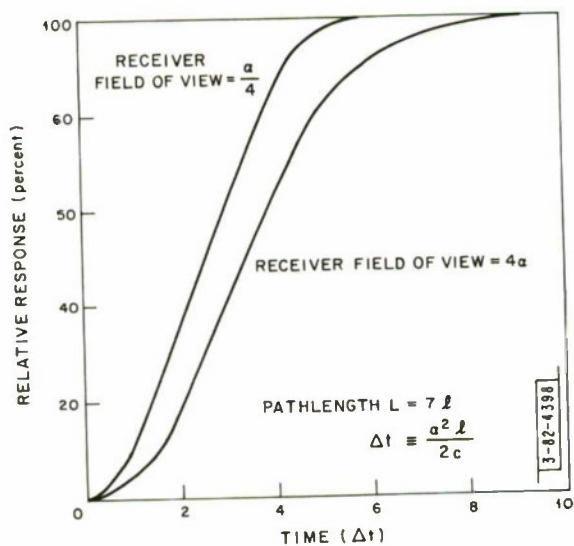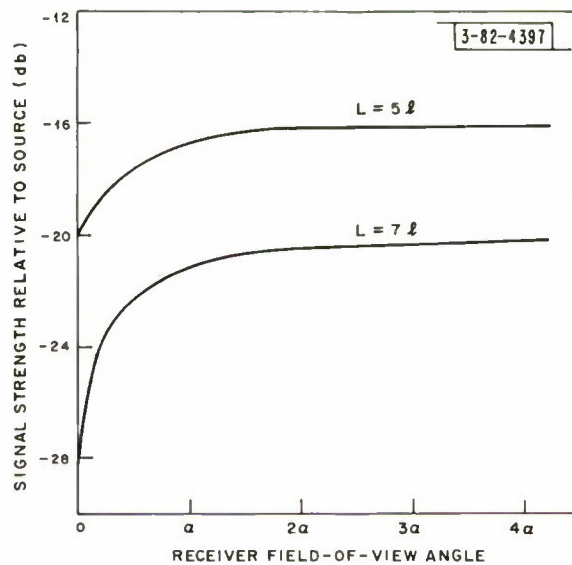Fig. A-7. Signal vs field-of-view characteristics.

Fig. A-8. Step-function response of multiple-scatter atmospheric channel.

Figure A-7 shows signal strength characteristics as a function of receiver field-of-view angle, in terms of α, the forward-scatter angle assumed in the elemental volume model. Curves are presented for pathlength and scatter density conditions of $L = 5\ell$ and $L = 7\ell$. It is seen that signal strength increases rapidly as the field-of-view is increased from small angles to angles several times the forward-scatter angle. This dependency becomes increasingly stronger with increasing scattering densities or pathlengths. For clouds and fog consisting of particles large compared to the wavelength, the forward-scatter angle α is expected to be of the order of several degrees.[14,15] Accordingly, desired field-of-view angles of the order of 5° to 10° are indicated. This indication is supported qualitatively by observations of spot lights in fog.

The final characteristic to be explored with the aid of our assumed atmospheric model is channel bandwidth as limited by the transit-time dispersion of multiple-scatter paths. Computations of channel response to a step function have been made, based on the atmospheric scatter model of Figs. A-3 and A-4. The computations consisted of tracing all the original incident flux through the multiple paths of the atmospheric model and of keeping an account of the incremental pathlengths traversed by each and every multiple-scattered ray.

Step-function responses for two values of receiver field-of-view angle corresponding to $\alpha/4$ (narrow field-of-view) and 4α (wide field-of-view) are given in Fig. A-8. In general, wider field-of-view receiver systems exhibit slower step-function responses with long tails resulting from the relatively few, but appreciably longer, multipaths. Risetime responses (10 to 90 percent) for a pathlength of seven mean paths taken from the computed curves of Fig. A-8 are:

$$\text{wide-angle } (4\alpha) \text{ system} = 4.5 \, \Delta t$$
$$\text{narrow-angle } (\alpha/4) \text{ system} = 3.3 \, \Delta t$$

where

$$\Delta t \equiv \frac{\alpha^2 \ell}{2c} \, (\text{nsec})$$

and

$$\alpha \equiv \text{forward-scatter angle (radians)}$$
$$\ell \equiv \text{mean path (feet)}$$
$$c \equiv \text{velocity of light} \simeq 1 \, \text{ft/nsec.}$$

Thus, we find a trade-off between signal strength and risetime response determined by receiver field-of-view.

If we assume a value of

$$\sigma = 2 (\text{KM}^{-1})$$

then

$$\ell = 1640 \text{ feet}$$

and the total pathlength

$$L = 2.2 \text{ miles.}$$

From the very few applicable theoretical calculations and rigorous experimental measurements of the volume scatter function, including small angles through $\varphi = 0$, for conditions of clouds and fog,[14,15] we assume what we believe may be high and low values for the forward-scatter

angle of the abstracted mean path volume scatter function.   Accordingly, for

$\alpha = 5°$

wide-angle system risetime = 29 nsec

small-angle system risetime = 21 nsec

and for

$\alpha = 1°$

wide-angle system risetime = 1.1 nsec

small-angle system risetime = 0.8 nsec

Thus, we may expect to find, for pathlengths up to seven mean paths through clouds and fog, channel bandwidths of tens to hundreds of megacycles.

Some support for the validity of the expected channel bandwidths derived in the foregoing analysis is seen in the results of field measurements described in Sec. VIII-B of this report. The pertinent test consisted of risetime-response measurements of pulses propagated over a 1.8-mile path in moderate snow and fog when the visibility was 0.6 mile.   A nominally narrow beamwidth laser source was employed with a nominally narrow field-of-view receiver.   Scatter conditions were such that the signal strength was 12 to 14 db below clear-air path conditions. As discussed in Sec. VIII-B, the risetime response of the channel was approximately 5 nsec.

Finally, it is noted that the preceding analysis is amenable to computer solution.   In a computer procedure, the volume scattering element could be chosen sufficiently small to insure that multiple scattering therein was negligible.   Instead of representing the volume scatter function by a single set of vectors in two dimensions at small scattering angle α, a large number of scattered rays in three dimensions and at various scatter angles could be included; and instead of assuming an ideally collimated source, a number of source rays at very small forward angles could be included.   Solutions could be computed for any combination of values for the extinction coefficient, ratio of scattered to absorbed flux, receiver field-of-view, etc. However, the refinements offered by computer analysis can be realized, for this particular application, only when equally refined and thorough experimental measurements of the volume scatter function, including small angles through $\varphi = 0$, are available for conditions of clouds and fog.

APPENDIX B
APPLICATIONS OF MULTIPLE-LASER-ARRAY TECHNOLOGY

A number of applications of the multiple-laser-array technology are presented which are based on the feasibilities demonstrated by laboratory tests on simple arrays and on the analysis and field measurements of optical propagation through atmospheric paths.

A generalized form of a multiple-laser-array system is shown in Fig. B-1. The generalized system consists of multiple arrays (L_1, L_2 ... L_n), each composed of a number of identical series-connected laser elements and having distinct radiant wavelengths (λ_1, λ_2 ... λ_n), each driven by electronic generators (E_1, E_2 ... E_n) in accordance with desired signal inputs (S_1, S_2 ... S_n), and each laser element of the arrays connected through fiber bundles, in accord with the technology described in the body of this report, to the focal plane of an optics system. The fiber bundles abut the semiconductor laser faces and cover all active areas of the laser junctions. The active fibers abutting active laser face areas are selected and compose a smaller bundle which leads to the optics system.

In one application wherein maximum peak pulse power is desired at a certain wavelength and within the limits of power dissipation ability of the several array structures, identical pulse signals trigger identical electronic generators which synchronously drive the several arrays, all composed of laser elements having the same radiant wavelength. The selected active fibers from each and every laser element are combined at the focal point of an optics system. An intense, narrow beam having a pulse modulation in response to the input pulse signals is projected from the system. It is believed that the achievement of peak pulse powers of at least 100 times the power from a single laser element is within the state-of-the-art of the technology described in this report.

A high-power, pulse-modulated system, such as described above, would have particular application for narrow-band or low-pulse-rate optical scatter communications, optical radar, or optical beacons.

The input pulse signals which, in one application, may be applied to a system such as that depicted in Fig. B-1 compose a pulse-position-modulation scheme for conveying video-bandwidth signals. A video signal may be sampled at a rate (e.g., 10 Mpps) which is approximately twice the frequency of the highest component, as depicted in Fig. B-2. State-of-the-art electronics can convert the sampled amplitudes (A_1, A_2 ... A_n) into corresponding delays (d_1, d_2 ... d_n) in reference to the clock pulses. The clock pulse train and the pulse train composed of the position-modulated pulses may be applied simultaneously to signal inputs S_1 and S_2 of the system depicted in Fig. B-1. Alternatively, the clock pulse train may be transmitted for brief periods between line and frame scans.

The technology developed here provides for laser pulses of 5-nsec risetimes at rates of 10 Mpps. Field measurements over a 1.8-mile path, which was three times the visibility range, indicated a leading-edge dispersion of approximately 5 nsec. If, then, a pulse-position delay of 5 nsec is used to convey each level of original signal amplitude, no errors in demodulated signal amplitude will be introduced by propagation through the path. If a modest amount of amplitude noise is tolerable under the worst propagation conditions, then a pulse-position delay
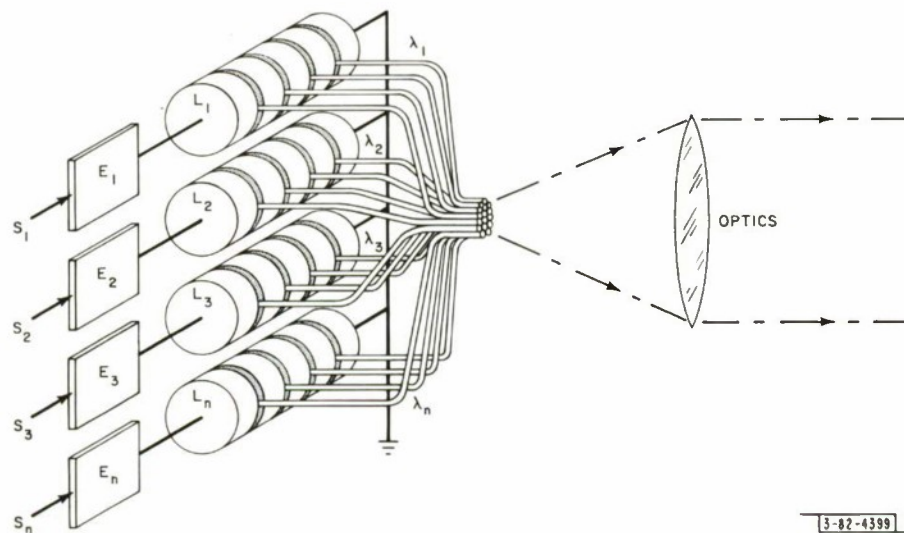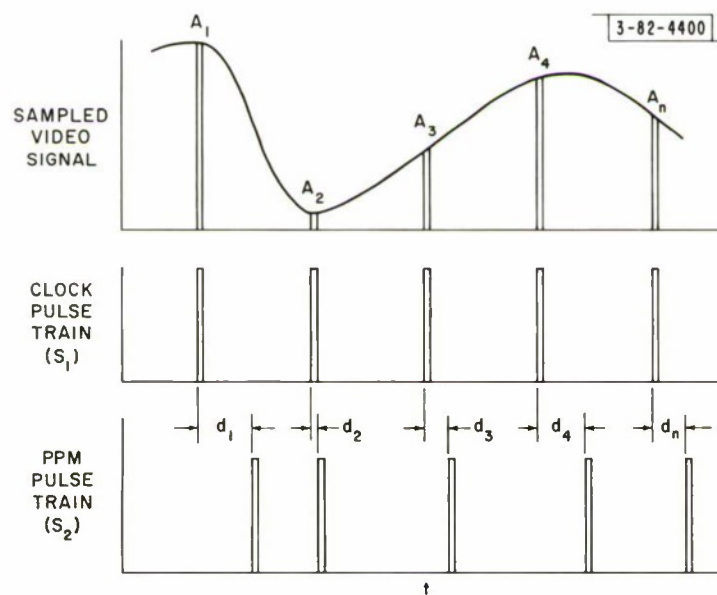
Fig. B-1. Generalized system of multiple-laser arrays.

Fig. B-2. Pulse-postian-modulatian signals.

64

of 2.5 nsec could be allotted for each amplitude level, and a video signal of 20 discrete amplitude levels could be conveyed by pulse-position modulations of 50 nsec. A system such as this would be adequate for conveying standard television video signals.

A more specialized system appears feasible for conveying very-wide-band information. One application involves transmitting the contents of an 8- × 11-inch printed page, with 10 lines/mm resolution and 10 levels of amplitude during the period of one second. These numbers were chosen to represent the highest data rates involved to permit a person in one location to scan rapidly through printed material in a remote location. The data rates of this application could be handled by time multiplexing of several PPM optical signals, using the embodiment shown in Fig. B-1. The video signal would be sampled at the rate of 24 Mpps, and the position-modulated pulses would be fed successively to the different inputs (S_1, S_2, S_3) of the multiple arrays of lasers. Thus, each laser array would be working at a pulse rate of 8 Mpps, and there would be no time overlap of pulses from the several arrays.

At the present time, nonlaser, IR emitting semiconductor diodes may be operated continuously, and it is hoped that CW laser semiconductor diodes,[16] will be available soon. Continuous operation capability permits frequency multiplexing of signals using the technology of the multiple arrays combined with fiber bundles. For this type of operation the electronic generators provide a forward DC bias with a superimposed RF subcarrier which is modulated — preferably frequency modulated. Each of the several laser arrays may employ a different subcarrier frequency.

Another technique for mutliplexing signals over one optical path may be termed "wavelength multiplexing." This technique is achieved by employing multiple arrays of lasers wherein the laser elements of one array have an identical radiant wavelength but different from that of the other arrays. The recent development of semiconductor lasers having a wavelength of choice within a wide spectral region[3] permits the multiplexing of as many signals as may be practically distinguished by the use of narrow-band filters at the receiver. Wavelength multiplexing would be a convenient means for conveying pulse code modulated signals.

A special case of a time-multiplexing method employs a system (see Fig. B-3) in which the fiber bundles leading from the individual arrays are positioned, in an orderly fashion, in the focal plane of the optics system such that the beam from one fiber bundle projects in a direction differing from the beam radiating from an adjacent fiber bundle by an angle which is approximately the half-power beamwidth from one bundle. Thus the orderly positioning of bundle ends in the focal plane, together with sequential excitation of the individual laser arrays, yields a projected beam which scans in accord with the sequential excitation. The scan pattern can be as complex as required for particular purposes and can be effected simply by the order of laser array excitation. One means for conveniently exciting the arrays so as to effect a scan is indicated in Fig. B-3. Use is made of the semiconductor laser's threshold level, together with coincidence drive pulses, to cause selective lasering action among the multiple elements or arrays. Each laser element or array of series-connected laser elements is electrically coupled to a secondary winding of a ferrite-core pulse transformer. Each transformer has two primaries which consist of a horizontal and a vertical drive line. A pulse, having a voltage less than the laser diode junction potential, applied to one line does not cause lasering action in any laser connected to that line. However, the coincidence of two pulses, one on a horizontal line and one on a vertical line, induces a voltage pulse of sufficient amplitude to drive the selected diode beyond laser
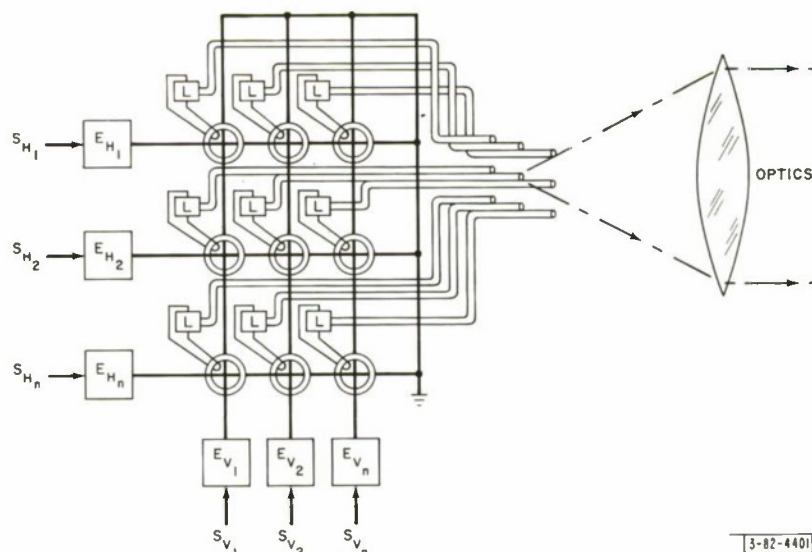
Fig. B-3. Electronically scanned laser array system.

threshold. Thus, scanning drives can be accomplished with an economy in the number of required pulse generators. One can envision a system of this sort employed to search and acquire a moving target and then to track and communicate with the target on a time-multiplexing basis.

Although some of the applications described above for arrays of semiconductor lasers combined with fiber optics are of long-range future potential, simpler applications are immediately practicable. The more immediate potentials are high-data-rate, short-range, fixed-point communications such as real-time-data transmission among remotely located sections of computer systems, wide-band optical links between hilltop microwave installations and subjacent communications centers, and low-data-rate beacons, telemetry, and radars between orbital and re-entry vehicles and ground stations.

The keys to the further development of communication applications of semiconductor lasers appear to be the cost and availability of lasers in substantial numbers. It is hoped that the development of multiple-laser-array technology, and the view presented here of their potential applications involving substantial numbers of laser elements, will assist in evaluating the future role of semiconductor lasers.

ACKNOWLEDGMENT

REFERENCES

1. R. J. Keyes and T. M. Quist, Proc. IRE (Correspondence) 50, 1822 (1962).

2. R. N. Hall, et al., Phys. Rev. Letters 9, 366 (1962); M. I. Nathan, et al., Appl. Phys. Letters 1, 62 (1962); T. M. Quist, et al., Appl. Phys. Letters 1, 91 (1962).

3. N. Halanyak and S. F. Bevaqua, Appl. Phys. Letters 1, 82 (1962); I. Melngailis, Appl. Phys. Letters 2, 176 (1963); K. Weiser and R. S. Levitt, Appl. Phys. Letters 2, 178 (1963).

4. R. H. Rediker, et al., Electronics 35, 44 (5 October 1962).

5. H. Nelson, et al., Proc. IEEE (Correspondence) 52, 1360 (1964); D. Karlsons, et al., Proc. IEEE (Correspondence) 52, 1354 (1964).

6. E. J. Chatterton, Proc. IEEE (Correspondence) 51, 612 (1963).

7. E. J. Chatterton (1960), publication not available. The general influence of atmospheric path geometry on the degree and the power spectral density of scintillation modulation was experimentally determined.

8. V. I. Tatarski, Wave Propagation in a Turbulent Medium (McGraw-Hill, New York, 1961).

9. H. B. Glen, The Optical Effects of Atmospheric Turbulence, Raytheon Company, Santa Barbara, California (April 1962).

10. R. J. Carbone and P. R. Langaker, Appl. Phys. Letters 4, 32 (1964).

11. B. Galdstein and R. Weigand, Proc. IEEE (Correspondence) 53, 195 (February 1965).

12. Solid State Research Reports, Lincoln Laboratory, M. I. T. (1962:4), DDC 400709, H-491; (1963:1), DDC 413089, H-517; (1963:3), DDC 427340, H-554; (1963:4), DDC 435023, H-573; (1964:1), DDC 601830, H-587.

13. W. E. K. Middleton, Vision Through the Atmosphere (University of Toronto Press, Toronto, Ontario, 1958), pp. 12-17.

14. B. S. Pritchard and W. G. Elliott, J. Opt. Soc. Am. 50, 191 (1960).

15. D. Deirmendjian, Electromagnetic Scattering (Pergamon Press, New York, 1963), p. 171.

16. J. C. Marinace, IBM J. Research Develop. 8, 543 (November 1964).

DOCUMENT CONTROL DATA - R&D

(Security classification of title, body of abstract and indexing annotation must be entered when the overall report is classified)

1. ORIGINATING ACTIVITY *(Corporate author)*	2a. REPORT SECURITY CLASSIFICATION
Lincoln Laboratory, M.I.T.	Unclassified
	2b. GROUP None

3. REPORT TITLE

Optical Communications Employing Semiconductor Lasers

4. DESCRIPTIVE NOTES *(Type of report and inclusive dates)*

Technical Report

5. AUTHOR(S) *(Last name, first name, initial)*

Chatterton, Edward J.

6. REPORT DATE	7a. TOTAL NO. OF PAGES	7b. NO. OF REFS
9 June 1965	76	25

8a. CONTRACT OR GRANT NO. AF 19(628)-500	9a. ORIGINATOR'S REPORT NUMBER(S)
b. PROJECT NO. 627A	Technical Report 392
c.	9b. OTHER REPORT NO(S) *(Any other numbers that may be assigned this report)*
d.	ESD-TDR-65-232

10. AVAILABILITY/LIMITATION NOTICES

Distribution of this document is unlimited.

11. SUPPLEMENTARY NOTES	12. SPONSORING MILITARY ACTIVITY
None	Air Force Systems Command, USAF

13. ABSTRACT

   This report discusses the development of optical communications employing semiconductor lasers – both noncoherent and coherent. The large modulation bandwidth obtainable with these devices permits the development of frequency- and pulse-modulation communications systems which overcome scintillation noise produced by the turbulent atmosphere. Emphasis has been placed on the development of communications systems for 98-percent weather capability over short ranges, rather than fair-weather capability over long ranges. The development of supporting technology is presented in the areas of semiconductor lasers, photomultipliers, and frequency- and pulse-modulation electronic circuitry and components.

   Measurements of optical signals over a two-mile path under a full variety of weather conditions have permitted a comparative evaluation of AM, FM, and PM systems. The results show clearly the advantage of frequency modulation and pulse modulation. Measurements of pulses transmitted appreciably beyond the limits of visibility in snow and fog indicate a channel bandwidth, limited by scatter-multipaths, but of the order of 200 Mcps.

   An analysis is presented of multiple-scatter paths and system design considerations for these conditions.

   The technology is described for combining the outputs of arrays of semiconductor lasers through fiber optics. Applications of the technology are discussed for (1) high-power, pulse-modulation systems, (2) time-, frequency-, and wavelength-multiplexing systems, (3) very-high-resolution optical television systems, and (4) electronically scanned laser systems.

14. KEY WORDS

optical systems	multipaths	multiplexing equipment
semiconductor lasers	optical communications systems	fiber optics
communications systems	optical propagation	gallium arsenide
scattering	scatter communications	